



Membrane Shape at the Edge of the Dynamin Helix Sets Location and Duration of the Fission Reaction

Sandrine Morlot,^{1,2} Valentina Galli,¹ Marius Klein,² Nicolas Chiaruttini,¹ John Manzi,² Frédéric Humbert,¹ Luis Dinis,^{3,4} Martin Lenz,^{5,6} Giovanni Cappello,² and Aurélien Roux^{1,7,*}

¹Biochemistry Department, University of Geneva, 1211 Geneva, Switzerland

²Institut Curie, Centre de Recherche, CNRS, UMR 168, Physico-Chimie Curie; Université Pierre et Marie Curie, 75248 Paris, France

³Departamento de Física Atómica, Molecular y Nuclear, Universidad Complutense de Madrid, 28040 Madrid, Spain

⁴Grupo Interdisciplinar de Sistemas Complejos (GISC), 28040 Madrid, Spain

⁵James Franck Institute, University of Chicago, Chicago, IL 60637, USA

⁶University Paris Sud, CNRS, UMR 8626 LPTMS, Orsay 91405, France

⁷Swiss National Centre for Competence in Research Programme Chemical Biology, 1211 Geneva, Switzerland

*Correspondence: Aurelien.roux@unige.ch

<http://dx.doi.org/10.1016/j.cell.2012.09.017>

SUMMARY

The GTPase dynamin polymerizes into a helical coat that constricts membrane necks of endocytic pits to promote their fission. However, the dynamin mechanism is still debated because constriction is necessary but not sufficient for fission. Here, we show that fission occurs at the interface between the dynamin coat and the uncoated membrane. At this location, the considerable change in membrane curvature increases the local membrane elastic energy, reducing the energy barrier for fission. Fission kinetics depends on tension, bending rigidity, and the dynamin constriction torque. Indeed, we experimentally find that the fission rate depends on membrane tension *in vitro* and during endocytosis *in vivo*. By estimating the energy barrier from the increased elastic energy at the edge of dynamin and measuring the dynamin torque, we show that the mechanical energy spent on dynamin constriction can reduce the energy barrier for fission sufficiently to promote spontaneous fission.

INTRODUCTION

Membrane fission is an essential step in membrane traffic, as it separates membrane cargoes from donor compartments. It is the inverse reaction to fusion. In many of the various fusion events in cells, a single type of machinery, the SNAREs, mediate the collapse of membranes. The general principle of the SNAREs mechanism is that the energy spent in the assembly of the SNARE complex overcomes the energy barrier to fusion by generating a hemifusion intermediate, also called the “stalk intermediate” (Kozlovsky and Kozlov, 2002). The stalk intermediate is a structure where the cytosolic leaflets of the two membrane compartments are fused into one, whereas the luminal

leaflets are still separated. In the case of fission, different machineries mediate the separation of two compartments depending on the cellular context: dynamin during endocytosis; endosomal sorting complex in retrograde transport-III (ESCRT-III) in multivesicular body biogenesis, cytokinesis, and viral budding (Hurley and Hanson, 2010). Small GTPases (Sar1, Arf1) involved in the initiation of the coat proteins (COPs)-dependent Golgi trafficking have also been recently implicated in the fission reaction of the COPs (Fromme et al., 2007). However, in all these fission reactions, it is not known whether the different machineries mediate fission on the basis on the same principle, mostly because physical understanding of how fission is mediated is lacking. By analogy to fusion, it has been, however, suggested that they operate through a similar stalk intermediate (Kozlovsky and Kozlov, 2003). Here, we focused on the physics of membrane fission, taking the dynamin system as a model in which the biochemistry is arguably better characterized than in other systems.

Dynamin has been biochemically and genetically implicated in fission of endocytic vesicles (Ferguson and De Camilli, 2012). It is a GTPase that polymerizes into helical collars at the neck of clathrin-coated pits (CCPs). The helical structure of dynamin immediately suggested that fission could be driven by a constriction of the helix.

When assembled in absence of guanosine triphosphate (GTP), the nonconstricted dynamin helix surrounds a membrane tube with a radius, R_u , of 10 nm (Chen et al., 2004; Danino et al., 2004). Upon GTP hydrolysis, a conformational change of dynamin at the dimer and the polymer levels (Chappie et al., 2011; Faelber et al., 2011; Ford et al., 2011) constricts the membrane (Danino et al., 2004; Sweitzer and Hinshaw, 1998). Constriction correlates with a reduction of the helix radius, itself reflected by a reduction of the number of dimers per helix turn from 14 to 13 (Chappie et al., 2011) and torsion. This torsion of the entire helical polymer can be monitored by live imaging (Roux et al., 2006). Early models (Hinshaw and Schmid, 1995; Takei et al., 1995) proposed that constriction was sufficient to break the neck, as constriction would proceed until fission is fully

completed. More recent data have modified our understanding of the possible role of constriction in dynamin-mediated membrane fission: (1) dynamin cryoelectron microscopy images and 3D reconstruction showed that the polymer can constrict down to a constriction radius, R_c , of 4–5 nm (Danino et al., 2004), filled with a tubular membrane (2 nm thick) that surrounds a water lumen (2–3 nm) (Chappie et al., 2011). These structural data support the idea that dynamin does not reach the hemifission state by constriction. (2) GTP-mediated constriction (Danino et al., 2004) and torsion (Roux et al., 2006) do not lead to fission unless the tube is both attached to the substrate (Danino et al., 2004) and subjected to longitudinal tension (Roux et al., 2006). These results showed that membrane constriction is not sufficient for fission and also suggested that mechanical parameters of the membrane (tension, bending rigidity) could play role in controlling fission.

Theory of membrane mechanics links the elastic energy, E_{el} , of the membrane to its shape via the Canham-Helfrich equation (Helfrich, 1973):

$$E_{el} = \sigma \Delta A + \int_A \frac{\kappa}{2} J^2 dA.$$

The first term of this equation ($\sigma \Delta A$) is the energy associated with membrane stretching, which depends on the membrane tension, σ , and the change in its surface area, ΔA . The second term is the energetic cost associated with membrane bending, a function of the local curvature, J (which characterizes the local shape of the membrane), multiplied by the membrane bending rigidity, κ , integrated over the whole membrane area, A . This rigidity depends on the lipid composition of the membrane. The Canham-Helfrich equation allows for calculating shapes and energies of lipid membranes in practically any conditions by measuring both membrane tension and rigidity.

As the dynamin helix constricts, it imposes a strong curvature on the membrane tube that it covers. This strong curvature has a high energetic cost. We thus reasoned that dynamin constriction could be significantly impeded by membrane elasticity, leading us to study how membrane mechanics influences the dynamin-mediated fission reaction.

In this study, we show that membrane fission is occurring at the frontier between the constricted dynamin coat and the bare membrane, a place where the important change in membrane curvature increases locally the elastic energy of the membrane. We further show that the energy barrier to fission is reduced by this local increase of membrane elastic energy, making fission spontaneously occur at the edge of dynamin. By setting rigidity (16 $k_B T$) and tension (from 10^{-5} to 5.10^{-4} N/m) and calculating the elastic energy difference between the unconstricted state (10 nm radius) of dynamin and the hemifission intermediate (3 nm radius), we estimate the energy barrier to fission to be of the order of 30–60 $k_B T$. By measuring the constriction strength, the torque of dynamin, we show that it is in the order of 700–1,000 pN nm, about 10 times larger than torques measured for other proteins. The huge value of the torque is, however, required to constrict the membrane to such extent. Moreover, we show that the mechanical energy spent by dynamin in constriction is sufficient to reduce the energy barrier to

fission by the same amount evaluated from the elastic energy of the membrane. Our results support a mechanism by which dynamin constricts fast, within a few hundreds of milliseconds, forcing the membrane to reach a high elastic energy state at the edge of the dynamin coat. The increased elastic energy of the membrane then triggers spontaneous fission at the edge of dynamin, which takes a few seconds.

RESULTS

Fission Occurs at the Edge of the Dynamin Coat

We adapted an *in vitro* assay (see Figure 1A) developed for the study of curvature-dependent lipid sorting (Sorre et al., 2009) and protein binding (Roux et al., 2010; Sorre et al., 2012). The assay is based on the generation of a membrane nanotube pulled out of a giant unilamellar vesicle (GUV) by means of optical tweezers. The membrane tension, σ , was set through aspiration of the GUV in a micropipette, allowing control over the dynamin-free tube radius, $r = \sqrt{\kappa/2\sigma}$. Using a second micropipette, we injected a mix of fluorescent Alexa-488 dynamin 1/nonfluorescent dynamin 1 in the vicinity of these nanotubes (see *Experimental Procedures*). In the absence of GTP, nucleation of dynamin seeds onto the nanotube, but no fission, was observed (Roux et al., 2010; data not shown). When GTP was added along with dynamin, small dynamin seeds formed along the tube, and membrane fission subsequently occurred (see Figure 1B; *Movie S1* available online). As previously described (Roux et al., 2006), the tube retracted rapidly following the first break, and no further break was observed. Using fast dual-color confocal imaging (see *Extended Experimental Procedures*), we observed that fission occurred at the edge of dynamin domain in 90% ($N = 10$) of the events (see Figures 1C and S1; *Movie S2*). Indeed, after fission, one extremity of the broken tube was covered with dynamin, whereas the other one was not (Figures 1C and S1; *Movie S2*). No fission was observed in the uncoated regions of the tube.

We hypothesized that the considerable change of curvature from the highly constricted dynamin-coated part to the less curved bare tube could favor fission. We were thus prompted to look at the efficiency of fission at the connection between the tube and the GUV, where the change in curvature is even more dramatic. Indeed, most of the fission events occurred at the boundary between the tube and the GUV (38%) or at the boundary between the tube and the bead (36%) ($N = 44$; Figures 1D and 1E; *Movie S3*). It is worth noting that shapes of the membrane at both connections are similar, as the membrane-bead adhesion patch is much larger (several hundreds of nanometers) than the size of the tube in this assay (Koster et al., 2005). Dynamin nucleation was homogeneous along the tube axis (Figure 1D, blue curve), indicating that this higher probability of fission was not due to preferential nucleation of dynamin at the bead, at the GUV, or on the parts of the nanotube adjacent to them but consistent with an influence of the local membrane shape (Figure 1F).

The Membrane Shape at the Dynamin-Membrane Edge Facilitates Fission

We then calculated the shape of the membrane at the edge of the constricted dynamin tube (hereinafter called the

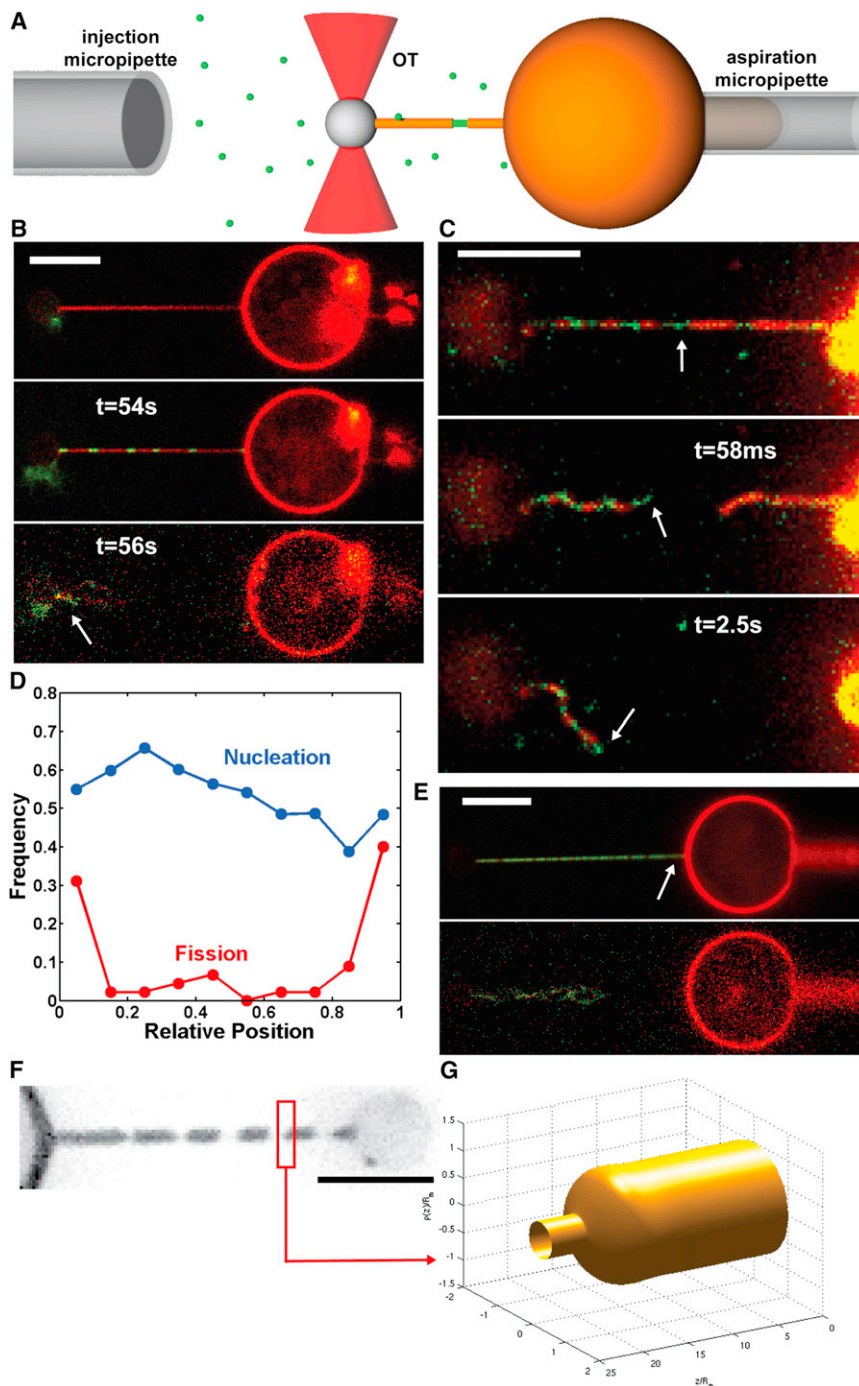


Figure 1. Localization of Fission Events at Dynamin-Membrane Edges

(A) Schematic drawing of the experimental set-up. A micropipette (right) sets the GUV's tension. A membrane nanotube is extracted from the GUV via a microbead trapped in optical tweezers (red cones). A second micropipette (left) injects locally dynamin and GTP.

(B) Confocal pictures of a GUV labeled with BodipyTMR-PI(4,5)P₂ (red channel) and dynamin labeled with Alexa 488 (green channel); see also [Movie S1](#). Top: Membrane nanotube before injection of dynamin + GTP. Middle: Nanotube partially coated with dynamin after injection of dynamin + GTP. Bottom: Fission 56 s after start of polymerization. Remaining tube is still attached to the bead (white arrow). Scale bars, 5 μm.

(C) Images from dual-color spinning disk confocal microscopy. Top: tube before fission. Middle: Same tube 58 ms after fission. Bottom: Same tube 2.5 s after fission. After fission, extremity of the left stump is covered with green dynamin, whereas the right stump is uncoated, showing that fission occurred at the edge between a seed of dynamin (white arrows) and the dynamin-free membrane nanotube (see also [Figure S1](#) and [Movie S2](#)). Scale bars, 5 μm.

(D) Frequency of dynamin nucleation (blue) and fission (red) along the nanotube. Position is normalized so that 0 and 1 are, respectively, the bead boundary and the connection between the tube and the GUV. N = 44 tubes.

(E) Confocal pictures of a GUV and a dynamin-coated nanotube as shown in (B) (see also [Movie S3](#)). Nothing remaining of the tube is seen on the GUV, showing that fission occurred at the connection between the tube and the GUV (white arrow). Scale bars, 5 μm.

(F) Fluorescence image of a membrane tube constricted by dynamin in presence of GTP (TMR-PE). Scale bars, 5 μm.

(G) Calculated shape a single dynamin-membrane edge by simulations.

"dynamin-membrane edge"). By setting the constriction radius R_c , σ , and κ (see [Extended Experimental Procedures](#)) and numerically minimizing the elastic energy of the membrane, we can calculate the shape of the dynamin-membrane edge ([Figures 1F and 1G](#)). The funnel shape of the dynamin-membrane edge is associated with a local increase in elastic energy that can be estimated numerically ([Figure 2B](#)) ([Shlomovitz et al., 2011](#)). This elastic energy depends on the ratio $\alpha = R_m/R_c$, where

wherever the membrane reaches a hemi-fission state, when the membrane radius shrinks below a threshold $R_i \sim 3$ nm ([Kozlovsky and Kozlov, 2003](#)), comparable to the membrane thickness (see fission intermediate in [Figure 2A](#)). The existence of such hemifission intermediate is supported by the experimental fact that fission is nonleaky ([Bashkirov et al., 2008](#)). Reaching an intermediate state with such a strongly curved membrane is a rare event and must thus be the rate-limiting step of membrane

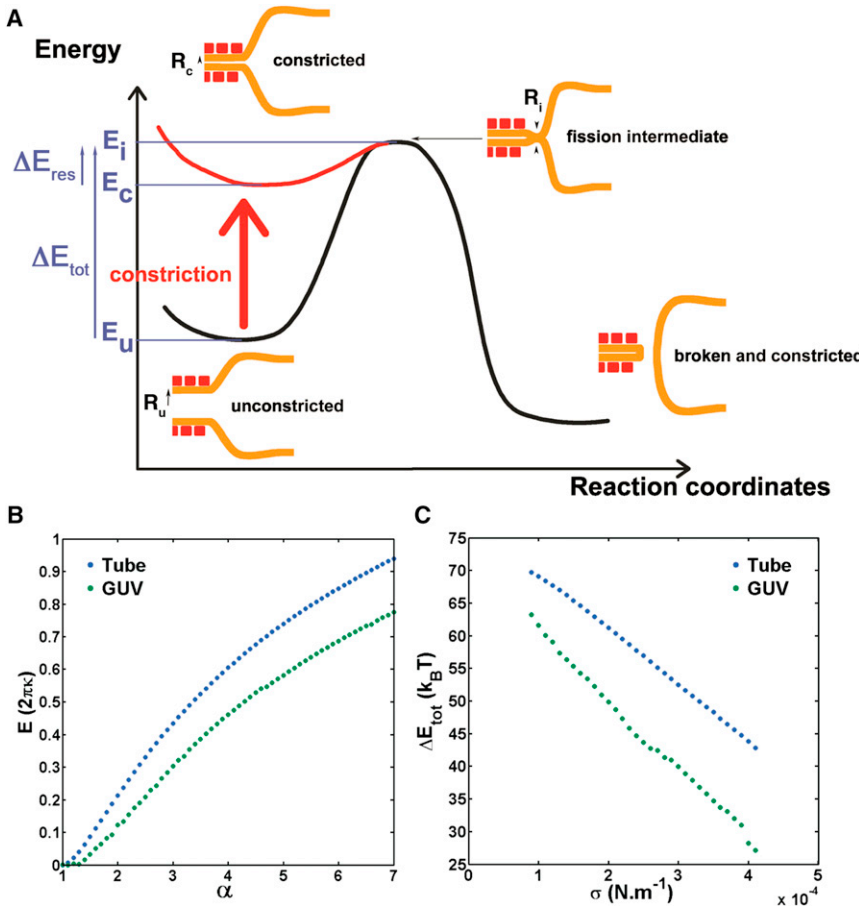


Figure 2. Energy Landscape of Dynamin-Mediated Fission

(A) Mechanism and associated energy landscape for dynamin-mediated fission reaction. Intermediate state corresponds to hemifission, in agreement with experiments using lysolipids shown in Figure S2.

(B) Energy of the neck joining the bare membrane tube with the dynamin-coated tube (blue) and energy of the neck joining a GUV or bead to a dynamin-coated tube (green) as a function of $\alpha = R_m/R_c$ with R_m as the radius of the dynamin-free tube and R_c as the radius of the constricted dynamin-coated tube.

(C) Total energy barrier for fission within the lipid tube (blue) or in the GUV-dynamin or bead-dynamin edge (green) as a function of tension for $\kappa = 16 k_B T$ and $R_i = 3 \text{ nm}$, $R_u = 10 \text{ nm}$.

fission. We propose that, by constriction of dynamin, the elastic energy of the membrane increases most at the edge of the dynamin coat, thereby reaching the constricted state (Figure 2A). Then thermal fluctuations of the membrane edge would allow spontaneous fusion of the inner layer of the tube, reaching the hemifission state. Since the energy of the intermediate state E_i and of the unstricted state E_u corresponds to the elastic energy of the membrane at the edge of dynamin, the full energy barrier is $\Delta E_{\text{tot}} = E_i - E_u$ (see Figure 2A).

We numerically estimated the magnitude of the energy barrier ΔE_{tot} in two cases: (1) for the membrane edge connected to the bead or GUV; and (2) for the membrane edge connected to the bare tube. For (1), $\Delta E_{\text{tot}} = 20-65 k_B T$, and for (2), $35-70 k_B T$ (Figure 2C; $k_B T$ is the thermal energy). These values are close to previous theoretical estimations for the fission energy barrier (Kozlovsky and Kozlov, 2003). The actual value of the barrier depends on membrane tension (see Figure 2C) and rigidity (data not shown). Also, as shown in Figure 2C, we predict that the energy barrier is smaller close to the bead or vesicle, thus accounting for a higher fission probability there (Figure 1D). We further estimated the probability to break close to the bead or GUV from the difference of these energy barriers (see Extended Experimental Procedures). Considering the range of tensions we have in our experiments (10^{-6} N/m - 10^{-4} N/m), we found this

probability to be between 70% and 95%, consistent with the above experimental value of $38 + 36 = 74\%$.

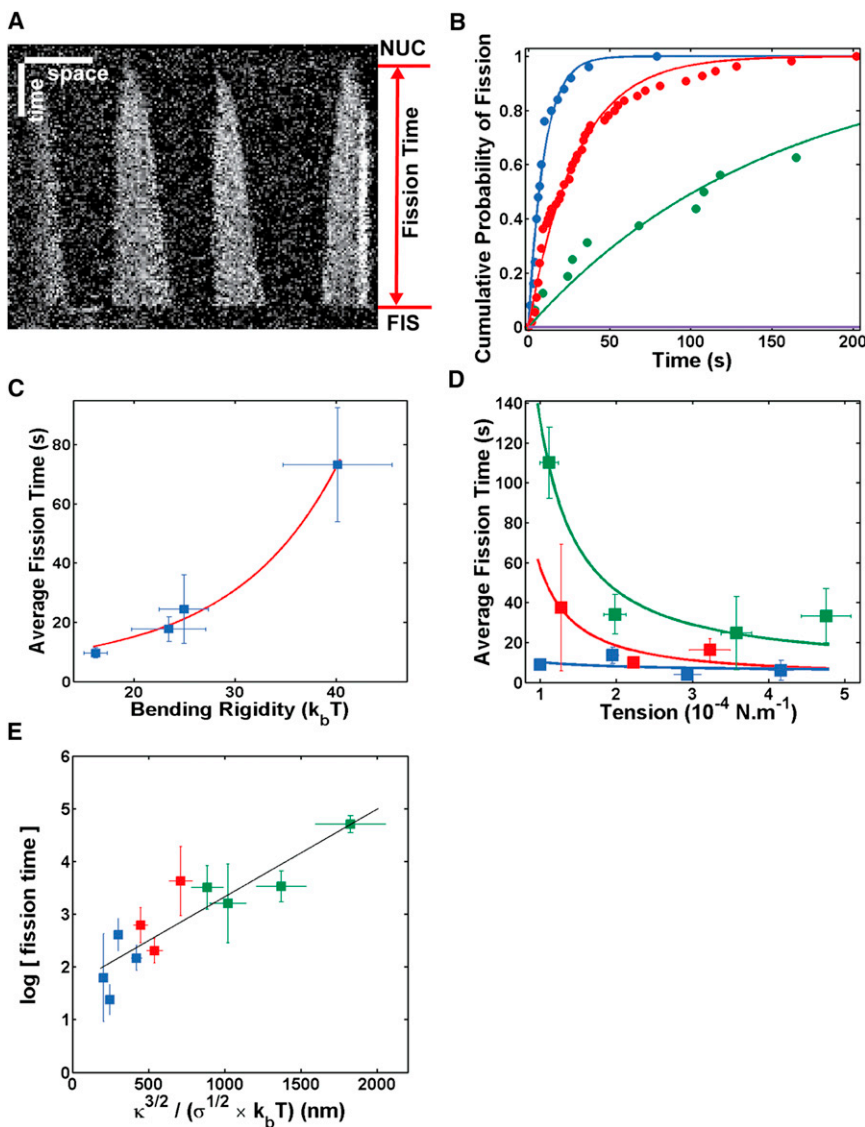
To further test the role of membrane elasticity in dynamin-mediated fission, we used our model to estimate the expected dependence of the average fission time, $\langle t_f \rangle$, with membrane tension and bending rigidity. According to the model (see Figure 2A), after constriction, fission at the dynamin-membrane edge is spontaneous and the residual energy barrier after constriction, $\Delta E_{\text{res}} = E_i - E_c$ is, this way, small enough to be overcome by thermal fluctuations of the

membrane (see Figure 2A). If after constriction, fission is thermally activated, $\langle t_f \rangle$, should satisfy a simple Arrhenius equation, $\langle t_f \rangle = \tau e^{\Delta E_{\text{res}}/k_B T}$, where $\tau \sim 1 \text{ ns}$ is the typical time scale of the membrane tube thermal fluctuations. By taking a linear approximation for the elastic energy of the edge with the curvature of the constricted dynamin tube ($1/R_c$), we find (see Extended Experimental Procedures):

$$\langle t_f \rangle \approx \tau \exp\left(\frac{b \kappa^{3/2}}{\sqrt{\sigma}} / k_B T\right), \quad (\text{Equation 1})$$

where b is a constant that depends on R_i and R_c ; σ , membrane tension; and κ , membrane rigidity.

We experimentally validated Equation 1 by studying how long it takes for dynamin to break membrane tubes. As dynamin and GTP are coinjected, we defined the fission time t_f as the time elapsed between nucleation of dynamin seeds and fission (see kymograph in Figure 3A). At $150 \mu\text{M}$ GTP, a physiological concentration of GTP (Otero, 1990), the average fission time $\langle t_f \rangle$ was $9.6 \pm 1.7 \text{ s}$, similar to the *in vivo* values (Taylor et al., 2011). The fission time decreased when the GTP concentration increases, with $\langle t_f \rangle$ at $1 \mu\text{M}$ GTP = $85.3 \pm 8.7 \text{ s}$ and $\langle t_f \rangle$ at 10 mM GTP = $6.2 \pm 0.8 \text{ s}$ (see Table S1). As a first test of our model, we verified that the fission times were exponentially distributed (Figure 3B; Table S1) as expected for a thermally

**Figure 3. Kinetics of Dynamin Fission**

(A) Kymograph. Fluorescence of Alexa488-dynamin along a membrane tube as a function of time. Dynamin polymerizes from four initial nucleation seeds until fission occurs. Fission time is measured as the time elapsed between start of polymerization (NUC) and fission (FIS). Here, $t_f = 168$ s.

(B) Cumulative probability of fission at four different conditions: [GTP] = 500 μ M (blue); [GTP] = 5 μ M (red); [GTP] = 375 μ M + [GTP γ S] = 125 μ M (green); and [GTP] = 250 μ M + [GTP γ S] = 250 μ M (purple). Circles, experimental points. Line, exponential fit $1 - \exp(-t/\tau)$. The fitted parameters, τ , for different GTP concentrations are listed in Table S1. Scale bars: horizontal, 5 μ m; vertical, 30 s.

(C) Bending rigidity dependence of fission time. Blue squares and bars: experimental points, average + SEM. Red line: $y = a \cdot \exp(bx^{3/2})$. Different lipid compositions are used to obtain different bending rigidities; see Table S2.

(D) Tension dependence of fission time. Blue: $\kappa = 16.2 \pm 1.2$ kT [EggPC+PI(4,5)P₂]. Red: $\kappa = 25.0 \pm 2.4$ kT [EggPC + Cholesterol + PI(4,5)P₂]. Green: $\kappa = 44.8 \pm 5.1$ kT [Sphingomyelin+PI(4,5)P₂]. Squares and bars: experimental points, average + SEM. Lines, $y = a \cdot \exp(b/x^{0.5})$.

(E) Relationship between the log of fission time and $\kappa^{3/2}/\sigma^{1/2}$. Same color code as in (D). Squares and bars: experimental points, average + SEM. As predicted by our model, we observed a linear dependence (black line), linear fit: $y = a \cdot x + b$, $a = 1.17 \pm 0.42 \cdot 10^6$, $b = 0.59 \pm 0.27$, $R^2 = 0.82$.

activated, single-step process obeying Poisson statistics. We then verified that the dynamin-mediated fission reaction proceeds through a hemifission intermediate. Lysolipids, such as lysophosphatidylcholine (LPC), are known to inhibit fusion because their conical shape increases the hydrophobic mismatch in the stalk intermediate, increasing the energy barrier to fusion (Chernomordik and Kozlov, 2008). We found that 30% mol/mol LPC increased the average fission time to 48.8 ± 16 s, with 10% of the tubes not breaking after 300 s (see Figure S2). These results strongly support our assumption that dynamin-mediated membrane fission proceeds through a hemifission intermediate, similar to the stalk/hemifusion intermediate in fusion.

We next tested the dependence of the fission time with membrane tension and rigidity (see Equation 1). In our *in vitro* assay, membrane tension can be tuned by changing the aspiration pressure in the micropipette, and rigidity can be tuned by changing the lipid composition (see Table S2; Extended Experi-

mental Procedures). As expected, the fission time increased with membrane rigidity (Figure 3C), following $\exp(\text{constant} \times \kappa^{3/2})$ (see Equation 1). Dependence of the fission time with membrane tension compatible with the predicted relation in $\exp(\text{constant}/\sqrt{\sigma})$ was also observed (Figure 3D). The observed dependences of the fission time with tension and rigidity are in good agreement with our model, but our model also states that they should be the dominant membrane parameters controlling the fission time. Following this statement, we expected the logarithm of $\langle t_f \rangle$ to have a linear dependence with $\kappa^{3/2}/\sqrt{\sigma}$ (see Equation 1), which was experimentally verified (Figure 3E). We concluded that the dependences of the fission time with membrane tension and rigidity further show that the mechanical determinants of the membrane shape control the kinetics of the dynamin fission reaction.

The Dynamin Torque Is Sufficient for Constriction

The mechanism proposed earlier for dynamin-mediated fission reaction is strongly dependent on the ability of dynamin to constrict. We thus wondered if the constriction strength of dynamin was sufficient to constrict such membrane necks. As dynamin undergoes torsion during constriction, it generates a torque (see Figures 4A and S3C; Movie S4). Thus, the constriction

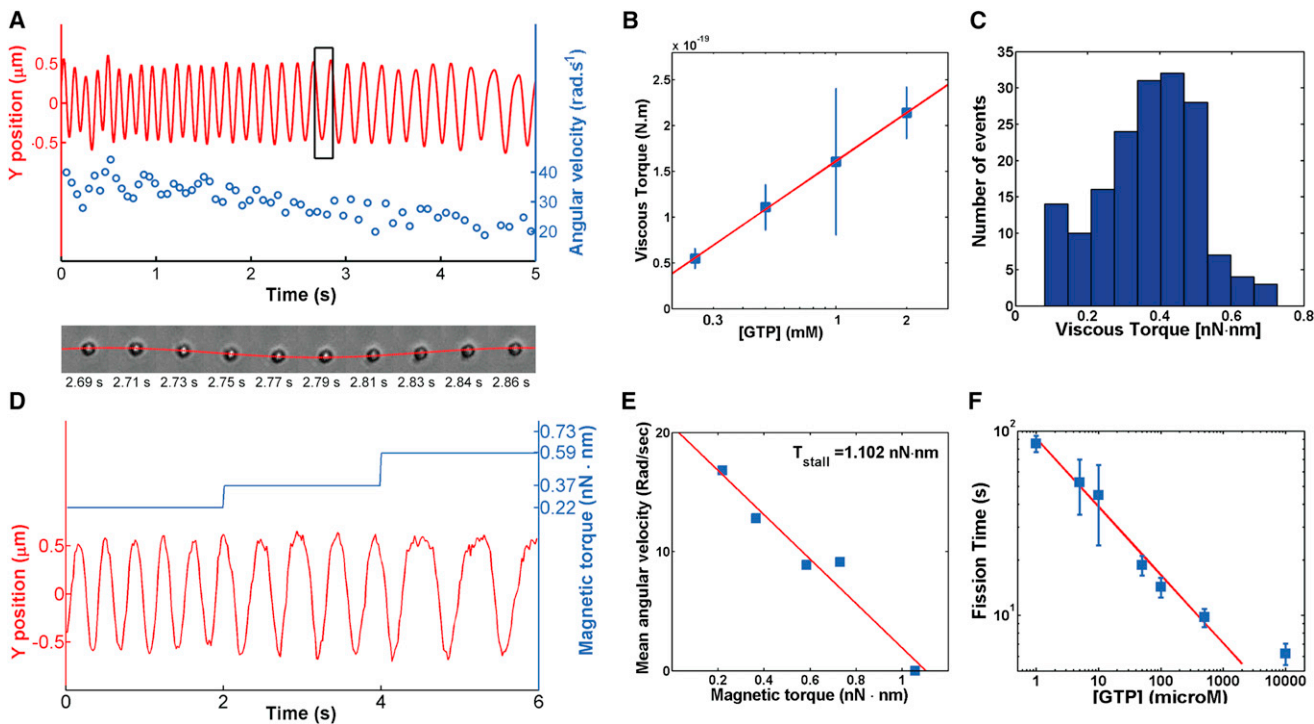


Figure 4. Torque Measurements

(A) Top: Y-position trace (red) and corresponding angular velocity values (blue) of a bead rotating around a membrane tube induced through dynamin twisting upon GTP hydrolysis. Bottom: Sequence of 10 frames of the bead performing exactly one rotation corresponding to the black rectangle. See also Movie S4.

(B) Linear dependence of the viscous torque with the log of the GTP concentration. Blue squares and bars: experimental points, average + SEM. Red line: linear fit, $y = a \times x + b$, $a = 1.43 \pm 1.00 \times 10^{-19}$, $b = 9.80 \pm 3.70 \times 10^{-20}$, $R^2 = 0.95$.

(C) Histogram of viscous torques measured from the fastest bead, as shown in Movie S4.

(D) Position relative to the axis of the tube of a magnetic, 695-nm radius streptavidin-coated bead rotating after addition of 1 mM GTP, and under the magnetic torque (blue; see text for explanations) generated by a magnetic field. The bead slows down as magnetic torque increases; see also Figure S3.

(E) Velocity of a rotating bead as the function of the magnetic torque. Bead stops at 1.1 nN·nm. See also Movie S5.

(F) [GTP]-dependence of fission time. Blue squares and bars: experimental points, average + SEM. Red line: linear fit, $y = a \times x + b$, $a = -0.37 \pm 0.07$, $b = 4.51 \pm 0.27$, $R^2 = 0.98$.

torque of dynamin must be strong enough to counteract membrane elasticity that widens the tube. In order to verify this, we measured the torque, Γ , exerted by dynamin during constriction by monitoring the position of beads of radius, r , attached to the dynamin coat. The beads rotated following GTP addition, allowing us to track the torsion of the dynamin coat (Morlot et al., 2010; Roux et al., 2006). Because of this fast motion, the beads incurred a viscous drag, which counteracted the torque generated by dynamin and limited the maximal angular speed. The viscous drag acting on a bead of radius r spinning around a linear axis is: $\Gamma_{\text{visc}} = 14\pi\eta r^3\omega$, where ω is the angular velocity of the bead and η is the viscosity of water. We used beads of 675 nm radius and measured an average angular speed of $\omega = 15.8 \pm 5$ rad/s at 2 mM GTP (Figure 4B), corresponding to an average torque of 214 ± 74 pN·nm. These beads are significantly slower than beads of 95–180 nm radii used in previous studies (~55 rad/s) (see Morlot et al., 2010; Roux et al., 2006) indicating that the viscous torque acting on the 675 nm beads is of the same order of the dynamin torque. Because the beads are rotating, the torque of dynamin is larger than the measured viscous torque. The highest value of the

viscous torque (730 pN·nm; see Figure 4C) obtained for the fastest bead is thus a closer underestimate of the dynamin torque. $\Gamma = 730$ pN·nm is 20 times larger than the torque developed by proteins twisting DNA (10–20 pN·nm for the recombinase RecA) (Lipfert et al., 2010) or the rotational motor F1 ATPase, which usually generate torques of 40 pN·nm (Yasuda et al., 1998).

We measured the maximum torque of dynamin (stall torque Γ_s) by attaching magnetic beads to dynamin-coated tubules and blocking their rotation with a magnetic field. After calibration of the set-up (see Extended Experimental Procedures and Figures S3A, S3B, S3D, and S3E), magnetic fields were translated into the magnetic torque experienced by the bead in the magnetic field. We found that beads stopped to rotate when magnetic torques exceeded 1,300 pN·nm at 1 mM GTP. Rotational movement started again upon switching off the magnetic field (Figure S3F; Movie S5), confirming that abrupt stop was due to magnetic field. We observed that the angular velocity of the bead decreased linearly with increasing intensities of the magnetic field (Figures 4D and 4E). Linear fits (Figure 4E) gave an average value of the stall torque of dynamin of $1,100 \pm 340$ pN·nm.

From the free energy of a dynamin-constricted tube (see [Extended Experimental Procedures](#)), we calculated that R_c is related to the dynamin torque by $R_c = R_u / (1 + (\Gamma R_u / 2\pi\kappa h))$, where $h = 13$ nm is the dynamin pitch. According to this relation, constriction from $R_u = 10$ nm to $R_c = 5$ nm radius would require a torque of approximately 500 pN.nm. We concluded that the large value of the dynamin torque measured earlier was necessary and sufficient for constriction of membrane necks.

Dynamin Mechanical Work Reduces the Energy Barrier to Fission

The mechanical work of dynamin is partially spent in reducing the energy barrier to fission. If our model is valid, this fraction of the mechanical work reduces significantly the energy barrier. The residual barrier ΔE_{res} should be in the range of a few $k_B T$. Thus, we expect the dynamin work to be of the same order of magnitude as the full barrier ΔE_{tot} estimated from the elastic energy of the membrane (discussed earlier). Theoretically, the fraction of the dynamin work can be subtracted from the energy barrier (see [Extended Experimental Procedures](#)), with $\Delta E_{res} = \Delta E_{tot} - c\Gamma\theta$, where $\Gamma\theta$ is the dynamin work ([Figure S3C](#); also discussed later). The fission time expression is then:

$$\langle t_f \rangle \approx \tau \exp(\Delta E_{tot} - c\Gamma\theta/k_B T), \quad (\text{Equation 2})$$

where c is a constant and θ is the angle by which the helix rotates for each GTP it hydrolyzes ([Figure S3C](#)). According to this definition, we can identify $\Gamma\theta$ as the work performed by the helix per hydrolyzed GTP. According to Equation 2, for each amount $\Gamma\theta$ of mechanical work performed per GTP, ΔE_{tot} is lowered by an amount $c\Gamma\theta$. Thus, c characterizes the efficiency with which mechanical work is used to lower the fission barrier. The work performed by dynamin upon the hydrolysis of one GTP is proportional to the difference in chemical potential between GTP and its hydrolysis products. Thus, for experimental concentrations of GTP, we expect:

$$\Gamma\theta = \xi k_B T \ln([GTP]) + \text{constant}, \quad (\text{Equation 3})$$

where the dimensionless number ξ is the yield of the conversion of chemical energy into work. As a consequence, the product $c\xi$ characterizes the efficiency with which dynamin uses chemical energy to lower the barrier to fission. Inserting Equation 3 into Equation 2, we finally find:

$$\ln(\langle t_f \rangle) = c\xi \ln([GTP]) + \text{constant}. \quad (\text{Equation 4})$$

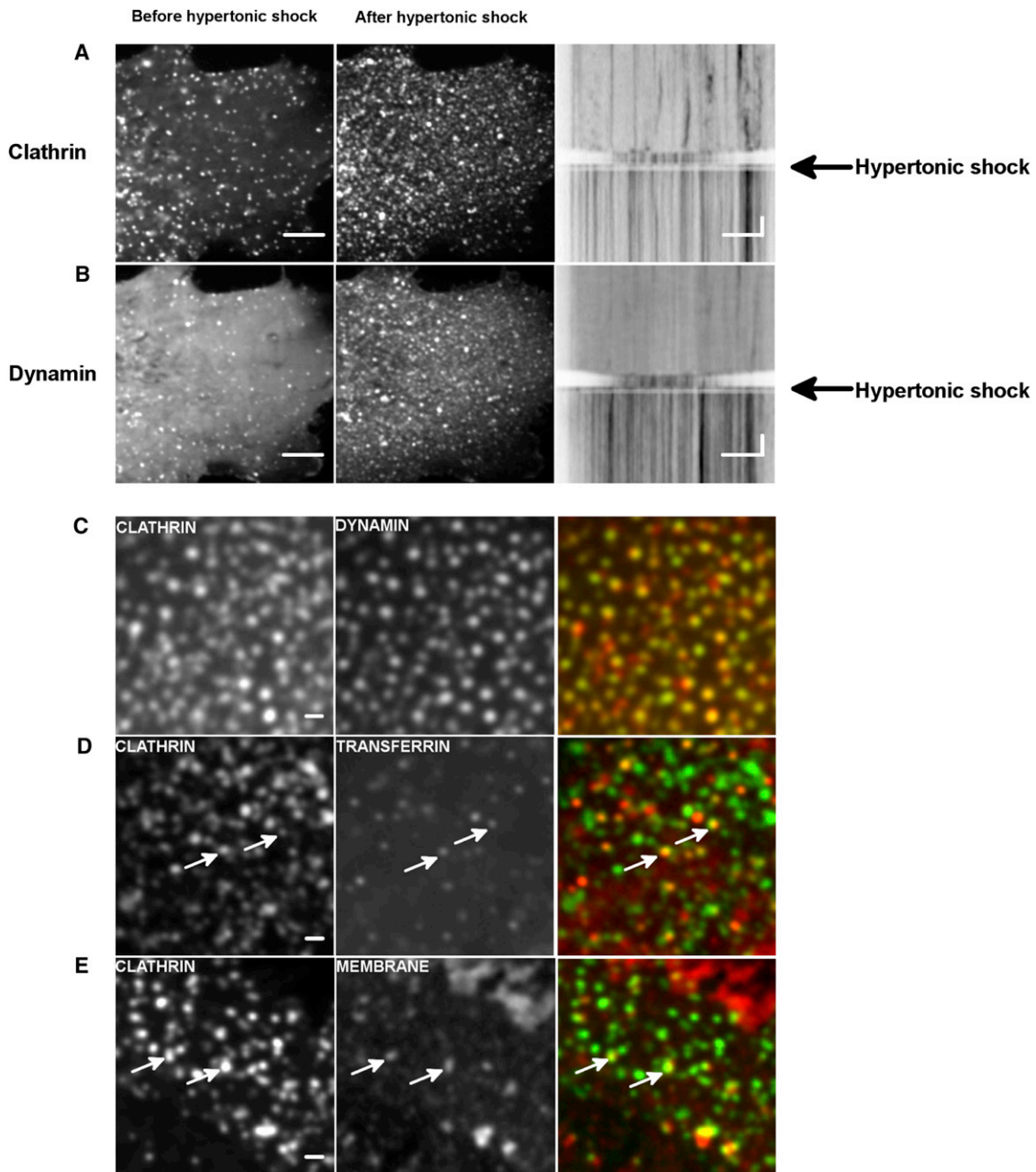
To validate this extended mechanochemical framework experimentally, we sought to verify the predicted GTP dependences and to characterize the efficiency $c\xi$. We first showed ([Figure 4B](#)) that the torque Γ depended linearly on $\ln([GTP])$, as expected from Equation 3. The slope allowed us to estimate $\xi/\theta = 34$. Knowing the full constriction angle θ_{full} from structural data ([Mears et al., 2007](#); 1/14 of a turn leads to $\theta_{full} = 2\pi/14 \approx 0.45$ rad), and assuming that $\xi = 1$, we could calculate the minimal number of hydrolyzed GTPs to reach full constriction $N = \theta_{full}/\theta = 34 \times 0.45 \approx 15$. We then measured the dependence

of the fission time on GTP concentration, yielding very good agreement with Equation 4 ([Figure 4F](#)) for values of GTP concentration lower than 10 mM. The experimental verification of Equation 4 validates our picture of the role of GTP hydrolysis in lowering the energy barrier to fission through a modification of the membrane shape. It is interesting that the slope of this curve gave $c\xi = 0.37 \pm 0.07$, meaning that over a large range of GTP concentrations, the reduction of the fission energy barrier represents 37% of the energy available from GTP hydrolysis. Knowing the minimal number N of GTP required for a full constriction of dynamin, we estimated the minimal energy E_{min} spent by dynamin in reducing the energy barrier to fission: One GTP delivers ~ 20 $k_B T$; thus, $E_{min} = \text{Fraction of chemical energy} \times N \times \text{Energy of hydrolysis of one GTP} = 37\% \times 15 \times 20k_B T \approx 111k_B T$. This value is of the same order of magnitude as the energy barrier ΔE_{tot} values (35–70 $k_B T$) estimated from the change in shape of the dynamin-membrane edge mediated by dynamin constriction. This simple calculation shows that dynamin through its constriction transfers enough energy to the membrane to significantly reduce the energy barrier to fission so that it becomes spontaneous at the dynamin-membrane edge.

Dynamin Reaction Kinetics Is Controlled by Membrane Tension In Vivo

We next studied if the shape of the dynamin-membrane edge could control the kinetics of dynamin fission in vivo. We aimed at reducing membrane tension and tracked the effect on the dynamics of CCP formation. We exchanged quickly the culture medium of Cos7 cells to medium containing 0.45 M sucrose ([Heuser and Anderson, 1989](#)) and followed the dynamics of clathrin-GFP by confocal imaging. As previously described ([Heuser and Anderson, 1989](#)), the rapid turnover of clathrin-GFP dots at the plasma membrane in Cos7 cells stopped within seconds after the shock ([Figure 5A; Movie S6](#)). The number of clathrin-GFP dots increased after the shock. These clathrin-GFP structures seemed to stay attached to the plasma membrane, suggesting a block of the clathrin-coated pits at the fission level. Consistently, dynamin-GFP followed the same behavior: More dots were seen after the shock ([Figure 5B; Movie S6](#)), without turnover (see kymograph in [Figure 5B](#)). Moreover, the clathrin-RFP structures perfectly colocalized with dynamin-GFP dots after the shock (~85%; see [Figure 5C](#)), showing that clathrin structures were blocked at the stage of dynamin ring formation. As the dynamics of clathrin bud are altered by overexpression of endocytic proteins, we tested the effect of hypertonic shock on genome-edited SKML-2 cells, where clathrin-RFP and dynamin-GFP are expressed at the same level as that of endogenous proteins ([Doyon et al., 2011](#)). When hypertonic medium was applied to these cells, the number of clathrin/dynamin dots increased, and their dynamic exchange was blocked (data not shown). As in Cos7 cells, clathrin-RFP dots colocalized with dynamin-GFP dots (see [Figure S4](#)).

We next verified that the clathrin dots blocked at the fission step were fully assembled CCPs. They indeed partially colocalized with transferrin, showing that cargo were present in these structures (see [Figure 5D](#)). As well, the plasma membrane lipophilic dye MASK (Invitrogen) showed a slightly increased signal in clathrin structures, reflecting the curved membrane of

**Figure 5. Block of Fission of CCPs by Hypertonic Shock**

(A) COS-7 cells transfected with mCTLA-mCherry before and after hypertonic shock; resulting kymograph that follows the time course before and after hypertonic shock.

(B) COS-7 cells transfected with DNM2-GFP before and after hypertonic shock; resulting kymograph that follows the time course before and after hypertonic shock. Scale bar, 5 μ m; time scale, 5 s. see also Movie S6.

(C) Colocalization of mCTLA-mCherry (red) and DNM2-GFP (green) in COS-7 cells after hypertonic shock; see also Figure S4.

(D) Colocalization of mCTLA-GFP (green) and transferrin (red) in COS-7 cells after hypertonic shock.

(E) Colocalization of mCTLA-GFP (green) and plasma membrane (red) in COS-7 cells after hypertonic shock. Scale bar, 1 μ m.

the bud (see Figure 5E). Taken together, these results strongly support the idea that many of the clathrin-coated dots frozen at the plasma membrane are fully assembled CCPs, blocked at the assembled dynamin stage, unable to break the membrane. These *in vivo* results are consistent with our *in vitro*

results: They show that a membrane tension decrease blocks dynamin-dependent endocytosis at the fission step, in a similar way than reduced membrane tension strongly delayed fission *in vitro*. Moreover, as previously reported (Boulant et al., 2011), we find that hypo-osmotic shock delays CCPs formation but

does not alter dynamin dynamics in the first few minutes after the shock (data not shown).

DISCUSSION

In this study, we first showed that dynamin-mediated fission occurs at the edge of the dynamin coat. Consistently, in mitochondrial fission, breakage was often observed at the boundary between the DNM1 ring and the rest of the mitochondria (Bleazard et al., 1999). We then showed that fission was facilitated at the dynamin-membrane edge because of the local membrane elastic energy increase due to considerable change in curvature. We next showed that not only the location but also the kinetics of the reaction is set by the shape of the membrane connecting the constricted tube to the bare part of the membrane. The constriction torque of dynamin and membrane elasticity parameters such as tension and bending rigidity that control the membrane edge shape thus act directly on the kinetics of dynamin-mediated membrane fission. Moreover, we showed in this study that the calculation of the energy barrier estimated from the shape of the membrane (from which we can estimate the elastic energy of the membrane) is in the range of 50–70 $k_B T$ and can be overcome by the mechanical work generated by dynamin during constriction (in the range of 100 $k_B T$). It is important to note that the contributions of the dynamin work, tension and rigidity to the kinetics of the fission reaction are different: Measured GTPase rate of dynamin in the assembled form (Praefcke and McMahon, 2004) suggests that the minimal amount of GTP required for full constriction is hydrolyzed within hundreds of milliseconds. Our previous study of the dynamics of dynamin constriction (Morlot et al., 2010) consistently showed that constriction should also happen within a few hundreds of milliseconds. As for nonlimiting GTP concentrations, fission takes a few seconds at least; our results are compatible with, first, (1) a fast constriction of dynamin, and then (2) a long delay to spontaneous fission of the constricted neck. Thus, at nonlimiting GTP concentrations (closer to *in vivo* situation), the kinetics of dynamin-membrane fission are expected to be primarily regulated by the elasticity of the membrane.

Indeed, we showed that, consistently with our *in vitro* results, clathrin-mediated endocytosis is blocked by reducing membrane tension *in vivo*. Also, *in vivo* (Taylor et al., 2011) and *in vitro* (this study and Bashkirov et al., 2008), typical fission times (a few seconds) are similar, with membrane tension values averaging 10^{-4} N/m, (for *in vivo* values, see Dai et al., 1997). Our finding that reduced membrane tension delays membrane fission is qualitatively similar to previous results showing the need of longitudinal tension for dynamin-mediated membrane fission (Roux et al., 2006). Consistently, when membrane tension is artificially kept low by using an excess of membrane reservoir, dynamin-mediated membrane fission takes several tens of seconds, close to a minute (Pucadyil and Schmid, 2008). Finally, we showed that increased membrane rigidity delays fission, which is consistent with previous findings where increased membrane rigidity inhibited fission (Bashkirov et al., 2008). These observations strengthen the idea that fission kinetics is controlled by elasticity of the membrane *in vivo*.

Recent studies (Bashkirov et al., 2008; Pucadyil and Schmid, 2008) have been undertaken to suggest that dynamin-mediated

fission could be triggered by GTP-induced depolymerization instead of constriction. Our results showing that fission occurs at the edge of the dynamin coat indicate that it requires partial coating of the membrane, which can be achieved either by partial polymerization of a bare membrane, or partial depolymerization of a fully coated membrane. However, in our experiments, we never observed depolymerization of the dynamin coat before (see Figure 3A) or after (see Figure 1C; $t = 2.5$ s) fission. Because in our experiments the optical resolution limit is above the size of a dynamin turn, we cannot exclude depolymerization restricted to a few turns. In the hypothesis that fission is mediated through depolymerization, it was predicted that long coats would have a reduced fission efficiency (Pucadyil and Schmid, 2008), as they would require more time to be fully depolymerized. In our experiments, we saw no dependence of the fission time with length of single dynamin seeds, from 150 nm to 10 μ m (see Figure S1B). Also, GTP energy was proposed to be spent in depolymerization rather than constriction (Bashkirov et al., 2008). The authors used conductance through dynamin-coated membrane tubes to measure their radii and found very small radii for assembled, nonconstricted dynamin (between 2 and 3 nm, 5–7 nm with membrane) when compared to the 10–11 nm radii found in other studies (Chen et al., 2004; Danino et al., 2004; Roux et al., 2010). When GTP was added, conductance increased before fission, suggesting disassembly. They concluded that GTP-induced depolymerization of dynamin could lead to spontaneous fission because of the narrow radius of assembled dynamin. This scenario becomes realistic for radii much below 10 nm, as tubules of 10 nm are stable. As the authors did not take into account the Debye length (Roux and Antonny, 2008), the screening distance of ionic charges (in the order of 1–2 nm), the conductance values of radii may not be accurate, which would explain discrepancy with other techniques (Chen et al., 2004; Danino et al., 2004; Roux et al., 2010; Sweitzer and Hinshaw, 1998; Takei et al., 1999). Thus, most probably, assembled dynamin makes tubules of 10 nm radius, which require further GTP-dependent constriction to be cut. In our present study, the good agreement between energetics of membrane constriction and dynamin torque work favors the hypothesis that GTP energy is primarily spent in constriction rather than in depolymerization.

In a broader perspective, the model presented here to explain the mechanism of dynamin function might show the important role of membrane elasticity for all fission reactions mediated by the constriction of a narrow membrane neck, as it is proposed for ESCRT-III-mediated fission (Fabrikant et al., 2009) and as it is the case in lipid phase separation (Roux et al., 2005). However, how constriction is performed and which energy source is used in other, dynamin-independent, fission reactions remains to be understood.

EXPERIMENTAL PROCEDURES

A full description of the methods is in the Extended Experimental Procedures.

Nanotube Pulling From GUV

GUVs were made by a modified protocol of the electroformation technique (Angelova et al., 1992; Roux et al., 2010). The aspiration of a GUV of radius R_{GUV} within a micropipette of radius $R_{pipette}$ allowed to set membrane tension: $\sigma = (1/2)(R_{pipette} \Delta P)/(1 - (R_{pipette}/R_{GUV}))$ (Evans and Rawicz, 1990).

A lipid nanotube was extruded from a micropipette-aspirated GUV containing 0.03% mol/mol of a biotinylated lipid (DSPE-PEG2000-Biotin, Avanti Polar Lipids, Alabaster, AL, USA) by moving away the pipette from an optically trapped, 3 μm diameter streptavidin-coated bead (Spherotech, Lake Forest, IL, USA) attached to the GUV prior to pulling. The fixed optical trap was custom-made and calibrated (see [Extended Experimental Procedures](#); stiffness, $k = 360 \text{ pN} \cdot \mu\text{m}^{-1} \cdot \text{W}^{-1}$). A mix of baculovirus purified human dynamin 1 (see [Extended Experimental Procedures](#) for purification details) and GTP (Roche Applied Science, Indianapolis, IN, USA) was injected in the vicinity of the lipid tube via a second micropipette. Two-color time-lapse acquisitions were performed with either a confocal microscopy (Eclipse C1 Nikon, Tokyo, Japan) or a spinning disk confocal (Intelligent Imaging Innovations, Denver, CO, USA).

Torque Measurement by Viscous Drag and Magnetic Field

Streptavidin beads (1.35 μm diameter streptavidin-coated, polystyrene beads, Spherotech, Lake Forest, Illinois, USA) are grafted onto biotinylated dynamin tubules formed from membrane sheets (see [Extended Experimental Procedures](#)) ([Morlot et al., 2010; Roux et al., 2006](#)). The beads rotate following GTP addition and resulting constriction of the dynamin coat ([Morlot et al., 2010; Roux et al., 2006](#)), experiencing a viscous torque $\Gamma_v = 14\pi\eta(R+r)^3\omega = \xi\omega$ ([Happel and Brenner, 1983](#)), where η is the viscosity of the surrounding fluid, R is the radius of the bead, r is the radius of the tubule, and ω is the angular spinning velocity. Differential interference contrast (DIC) and computer-based live recording of the rotating beads with a GUPPY camera (Allied Vision Technologies, Stadtdroda, Germany) allowed direct measure of the angular spinning velocity and estimation of the viscous torque from the aforementioned formula.

The stall torque, I_s , was measured by using magnetic beads (1.31 μm diameter streptavidin-coated, paramagnetic beads; Spherotech, Lake Forest, IL, USA), to which is applied an external torque via a variable electromagnetic field. This magnetic field was calibrated by two independent methods detailed in the [Extended Experimental Procedures](#).

Cell Transfections, Plasma Membrane Staining, Transferrin Uptake, and Hypertonic Shock

COS-7 cells were transfected using FuGENE-6 (Roche Applied Science, Indianapolis, IN, USA) with dynamin 2 fused to green fluorescent protein (GFP) (kindly provided by P. De Camilli; Howard Hughes Medical Institute [HHMI], Yale University) or mouse clathrin-light-chain fused to mCherry or GFP (kindly provided by C. Merrifield, Cambridge University, and by P. De Camilli, HHMI, Yale University). Cells were imaged 18 to 24 hr posttransfection in Leibovitz medium (GIBCO, Life Technologies, Paisley, UK). While imaging, the medium was changed with a hypertonic solution of 0.25 M sucrose in Leibovitz medium. Cell membrane staining was achieved by incubating cells for 5 min at 37°C with deep red Cell Mask (Molecular Probes, Life Technologies, Paisley, UK) before imaging. For Transferrin uptake assays, cells were starved in serum-deprived Dulbecco's modified Eagle's medium M-F12 for 30 min on ice, then incubated with 5 $\mu\text{g}/\text{ml}$ Alexa-fluor 594 Transferrin (Invitrogen, Grand Island, NY, USA) in hypertonic medium (0.25 M sucrose Leibovitz medium) for 3 min at RT. Cells were washed with hypertonic buffer before imaging.

SUPPLEMENTAL INFORMATION

Supplemental Information includes Extended Experimental Procedures, four figures, two tables, and six movies and can be found with this article online at <http://dx.doi.org/10.1016/j.cell.2012.09.017>.

ACKNOWLEDGMENTS

We thank David Drubin for sharing with us the SKML-2 cells. We thank Marcos González-Gaitán, for inspiring discussions and critical reading of the manuscript. We thank Pietro De Camilli, Jacques Prost, and Jean-François Joanny for thoughtful comments on this study. This work was supported by the Agence Nationale de la Recherche (Young Investigator Program Award No. JC08-317536 to A.R. and G.C.), Human Frontier Science Program Career

Development Award No. 0061/2008 (to A.R.), Young Investigator Research Grant No. RGY0076/2009-C (to A.R.), Swiss National Fund for Research Grant No. 31003A-130520/1 (to A.R.), the Société Académique de Genève, and the Swiss National Centre for Competence in Research Programme Chemical Biology. L.D. acknowledges financial support from Grant ENFASIS (FIS2011-22644, from the Spanish Government).

Received: May 10, 2012

Revised: July 6, 2012

Accepted: September 14, 2012

Published: October 25, 2012

REFERENCES

- Angelova, M.I., Soléau, S., Méléard, P., Faucon, J.F., and Bothorel, P. (1992). Preparation of giant vesicles by external AC electric fields. Kinetics and applications. *Prog. Colloid Polym. Sci.* 89, 127–131.
- Bashkirov, P.V., Akimov, S.A., Evseev, A.I., Schmid, S.L., Zimmerberg, J., and Frolov, V.A. (2008). GTPase cycle of dynamin is coupled to membrane squeeze and release, leading to spontaneous fission. *Cell* 135, 1276–1286.
- Bleazard, W., McCaffery, J.M., King, E.J., Bale, S., Mozdy, A., Tieu, Q., Nunnari, J., and Shaw, J.M. (1999). The dynamin-related GTPase Dnm1 regulates mitochondrial fission in yeast. *Nat. Cell Biol.* 1, 298–304.
- Boulant, S., Kural, C., Zeeh, J.-C., Ubelmann, F., and Kirchhausen, T. (2011). Actin dynamics counteract membrane tension during clathrin-mediated endocytosis. *Nat. Cell Biol.* 13, 1–10.
- Chappie, J.S., Mears, J.A., Fang, S., Leonard, M., Schmid, S.L., Milligan, R.A., Hinshaw, J.E., and Dyda, F. (2011). A pseudoatomic model of the dynamin polymer identifies a hydrolysis-dependent powerstroke. *Cell* 147, 209–222.
- Chen, Y., Zhang, P., Egelman, E., and Hinshaw, J.E. (2004). The stalk region of dynamin drives the constriction of dynamin tubes. *Nat. Struct. Mol. Biol.* 11, 574–575.
- Chernomordik, L.V., and Kozlov, M.M. (2008). Mechanics of membrane fusion. *Nat. Struct. Mol. Biol.* 15, 675–683.
- Dai, J., Ting-Beall, H.P., and Sheetz, M.P. (1997). The secretion-coupled endocytosis correlates with membrane tension changes in RBL 2H3 cells. *J. Gen. Physiol.* 110, 1–10.
- Danino, D., Moon, K.H., and Hinshaw, J.E. (2004). Rapid constriction of lipid bilayers by the mechanochemical enzyme dynamin. *J. Struct. Biol.* 147, 259–267.
- Doyon, J.B., Zeitler, B., Cheng, J., Cheng, A.T., Cherone, J.M., Santiago, Y., Lee, A.H., Vo, T.D., Doyon, Y., Miller, J.C., et al. (2011). Rapid and efficient clathrin-mediated endocytosis revealed in genome-edited mammalian cells. *Nat. Cell Biol.* 13, 331–337.
- Evans, E., and Rawicz, W. (1990). Entropy-driven tension and bending elasticity in condensed-fluid membranes. *Phys. Rev. Lett.* 64, 2094–2097.
- Fabrikant, G., Lata, S., Riches, J.D., Briggs, J.A., Weissenhorn, W., and Kozlov, M.M. (2009). Computational model of membrane fission catalyzed by ESCRT-III. *PLoS Comput. Biol.* 5, e1000575.
- Faelber, K., Posor, Y., Gao, S., Held, M., Roske, Y., Schulze, D., Haucke, V., Noé, F., and Daumke, O. (2011). Crystal structure of nucleotide-free dynamin. *Nature* 477, 556–560.
- Ferguson, S.M., and De Camilli, P. (2012). Dynamin, a membrane-remodelling GTPase. *Nat. Rev. Mol. Cell Biol.* 13, 75–88.
- Ford, M.G., Jenni, S., and Nunnari, J. (2011). The crystal structure of dynamin. *Nature* 477, 561–566.
- Fromme, J.C., Ravazzola, M., Hamamoto, S., Al-Balwi, M., Eyaid, W., Boyadjiev, S.A., Cosson, P., Schekman, R., and Orci, L. (2007). The genetic basis of a craniofacial disease provides insight into COPII coat assembly. *Dev. Cell* 13, 623–634.
- Happel, J., and Brenner, H. (1983). Low Reynolds Number Hydrodynamics: With Special Applications to Particulate Media (New York: Springer).

- Helfrich, W. (1973). Elastic properties of lipid bilayers: theory and possible experiments. *Z. Naturforsch. C.* 28, 693–703.
- Heuser, J.E., and Anderson, R.G. (1989). Hypertonic media inhibit receptor-mediated endocytosis by blocking clathrin-coated pit formation. *J. Cell Biol.* 108, 389–400.
- Hinshaw, J.E., and Schmid, S.L. (1995). Dynamin self-assembles into rings suggesting a mechanism for coated vesicle budding. *Nature* 374, 190–192.
- Hurley, J.H., and Hanson, P.I. (2010). Membrane budding and scission by the ESCRT machinery: it's all in the neck. *Nat. Rev. Mol. Cell Biol.* 11, 556–566.
- Koster, G., Cacciuto, A., Derényi, I., Frenkel, D., and Dogterom, M. (2005). Force barriers for membrane tube formation. *Phys. Rev. Lett.* 94, 068101.
- Kozlovsky, Y., and Kozlov, M.M. (2002). Stalk model of membrane fusion: solution of energy crisis. *Biophys. J.* 82, 882–895.
- Kozlovsky, Y., and Kozlov, M.M. (2003). Membrane fission: model for intermediate structures. *Biophys. J.* 85, 85–96.
- Lenz, M., Prost, J., and Joanny, J.-F. (2008). Mechanochemical action of the dynamin protein. *Phys. Rev. E Stat. Nonlin. Soft Matter Phys.* 78, 011911, PMID: 18763986.
- Lipfert, J., Kerssemakers, J.W., Jager, T., and Dekker, N.H. (2010). Magnetic torque tweezers: measuring torsional stiffness in DNA and RecA-DNA filaments. *Nat. Methods* 7, 977–980.
- Mears, J.A., Ray, P., and Hinshaw, J.E. (2007). A corkscrew model for dynamin constriction. *Structure* 15, 1190–1202.
- Morlot, S., Lenz, M., Prost, J., Joanny, J.F., and Roux, A. (2010). Deformation of dynamin helices damped by membrane friction. *Biophys. J.* 99, 3580–3588.
- Otero, A.D. (1990). Transphosphorylation and G protein activation. *Biochem. Pharmacol.* 39, 1399–1404.
- Praefcke, G.J., and McMahon, H.T. (2004). The dynamin superfamily: universal membrane tubulation and fission molecules? *Nat. Rev. Mol. Cell Biol.* 5, 133–147.
- Pucadyil, T.J., and Schmid, S.L. (2008). Real-time visualization of dynamin-catalyzed membrane fission and vesicle release. *Cell* 135, 1263–1275.
- Roux, A., and Antonny, B. (2008). The long and short of membrane fission. *Cell* 135, 1163–1165.
- Roux, A., Cuvelier, D., Nassoy, P., Prost, J., Bassereau, P., and Goud, B. (2005). Role of curvature and phase transition in lipid sorting and fission of membrane tubules. *EMBO J.* 24, 1537–1545.
- Roux, A., Uyhazi, K., Frost, A., and De Camilli, P. (2006). GTP-dependent twisting of dynamin implicates constriction and tension in membrane fission. *Nature* 441, 528–531.
- Roux, A., Koster, G., Lenz, M., Sorre, B., Manneville, J.-B., Nassoy, P., and Bassereau, P. (2010). Membrane curvature controls dynamin polymerization. *Proc. Natl. Acad. Sci. USA* 107, 4141–4146.
- Shlomovitz, R., Gov, N., and Roux, A. (2011). Membrane-mediated interactions and the dynamics of dynamin oligomers on membrane tubes. *New J. Phys.* 13, 065008. <http://dx.doi.org/10.1088/1367-2630/13/6/065008>.
- Sorre, B., Callan-Jones, A., Manzi, J., Goud, B., Prost, J., Bassereau, P., and Roux, A. (2012). Nature of curvature coupling of amphiphysin with membranes depends on its bound density. *Proc. Natl. Acad. Sci. USA* 109, 173–178.
- Sorre, B., Callan-Jones, A., Manneville, J.B., Nassoy, P., Joanny, J.F., Prost, J., Goud, B., and Bassereau, P. (2009). Curvature-driven lipid sorting needs proximity to a demixing point and is aided by proteins. *Proc. Natl. Acad. Sci. USA* 106, 5622–5626.
- Sweitzer, S.M., and Hinshaw, J.E. (1998). Dynamin undergoes a GTP-dependent conformational change causing vesiculation. *Cell* 93, 1021–1029.
- Takei, K., McPherson, P.S., Schmid, S.L., and De Camilli, P. (1995). Tubular membrane invaginations coated by dynamin rings are induced by GTP-gamma S in nerve terminals. *Nature* 374, 186–190.
- Takei, K., Slepnev, V.I., Haucke, V., and De Camilli, P. (1999). Functional partnership between amphiphysin and dynamin in clathrin-mediated endocytosis. *Nat. Cell Biol.* 1, 33–39.
- Taylor, M.J., Perrais, D., and Merrifield, C.J. (2011). A high precision survey of the molecular dynamics of mammalian clathrin-mediated endocytosis. *PLoS Biol.* 9, e1000604.
- Yasuda, R., Noji, H., Kinoshita, K., Jr., and Yoshida, M. (1998). F1-ATPase is a highly efficient molecular motor that rotates with discrete 120 degree steps. *Cell* 93, 1117–1124.

Supplemental Information

EXTENDED EXPERIMENTAL PROCEDURES

Materials

Egg L- α -phosphatidylcholine (EPC), brain sphingomyelin (BSM), L- α -phosphatidylinositol-4,5-bisphosphate (PIP₂), di-stearoyl phosphatidyl ethanolamine-PEG(2000)-Biotin (DSPE-PEG2000-Biotin), cholesterol and 1-stearoyl-2-hydroxy-sn-glycero-3-phosphocholine (Lyso PC) were purchased from Avanti Polar Lipids, Alabaster, Alabama, USA. BodipyTMR-PIP₂ (RedPIP₂) was purchased from Echelon Bioscience, Salt Lake City, Utah, USA, and Guanosine Triphosphate (GTP) from Roche Applied Science, Indianapolis, Indiana, USA. Five lipid preparations were used (molar percentage): 80% EPC + 19%PIP₂ + 1%RedPIP₂; 70% EPC + 10% BSM + 19%PIP₂ + 1%RedPIP₂ supplemented with 40% cholesterol; 80% EPC + 19%PIP₂ + 1%RedPIP₂ supplemented with 50% cholesterol; 80% BSM + 19%PIP₂ + 1%RedPIP₂ supplemented with 50% cholesterol and 50% EPC + 30% Lyso PC + 19% PIP₂ + 1%RedPIP₂. These five mixtures also contained 0.03% DSPE-PEG2000-Biotin.

Protein Purification

Recombinant human dynamin 1 was purified from Sf9 cells infected with recombinant baculovirus using the BD baculogold expressing system (BD Biosciences, Franklin Lakes, NJ USA). Dynamin was purified from cell lysate with the GST-tagged SH3 domain of rat Amphiphysin 1 as an affinity ligand as previously described (Stowell et al., 1999). Briefly, cells from twenty 150cm² flasks were re-suspended in 20 ml of Buffer A (20 mM HEPES pH 7.4, 100 mM NaCl, 1 mM EGTA, 1 mM DTT, 1% Triton X-100) supplemented with the protease inhibitor cocktail (cOmplete ULTRA Tablets, Roche Applied Science, Indianapolis, Indiana, USA) and homogenized with a 60 ml dounce. The lysate was centrifuged at 40krpm on a Ti70 rotor (Beckman-Coulter, Brea, CA), and the supernatant was incubated for 2 hr with glutathione beads to which 3-5 mg of purified GST-SH3 domain of rat Amphiphysin 1 were attached. Next, the beads were batch-washed with 150 ml of Buffer A without Triton X-100. Elution was done with high salt (20 mM HEPES, pH 7.4, 1.2 M NaCl, 1 mM MgCl₂). Unlabeled dynamin was dialyzed against storage buffer (20 mM HEPES, pH 7.4, 100 mM NaCl, 1 mM MgCl₂), concentrated using Amicon (50kDa CO), aliquoted, flash-frozen in liquid N₂ and stored at -80°C.

To fluorescently label dynamin, we dialyzed dynamin against PBS 50% glycerol. The labeling reaction was conducted using standard procedures (Alexa-488 protein labeling kit from Invitrogen, cat# A-10235). In some case, dynamin 1 was labeled with Alexa Fluor 488 C5 maleimide (Molecular Probes, Life Technologies, Paisley, UK). To attach streptavidin-coated microbeads to dynamin polymers, dynamin was conjugated to DSB-X Biotin C2-iodoacetamide (Molecular Probes, Life Technologies, Paisley, UK). Labeled dynamins were dialysed against storage buffer, aliquoted and kept at -80°C.

Nanotube Pulling from GUV

Lipid mix (0.5 mg/ml) was deposited on indium-tin oxide coated glass slides and dried 1h at 55°C to remove all solvents. GUVs were electroformed (1V, 10Hz) (Angelova et al., 1992; Stowell et al., 1999) for 1h at 55°C in a 200 mM sucrose solution then transferred in an observation chamber pretreated with Casein solution (2 mg/ml). GUVs were aspirated in a micropipette controlled with a motorized micromanipulator (MP-225, Sutter Instrument, Novato, California, USA) and a custom-made hydraulic system to control aspiration pressure ΔP and to set the tension: $\sigma = 1/2(R_{\text{pipette}}\Delta P/(1 - R_{\text{pipette}}/R_{\text{GUV}}))$ where R_{pipette} and R_{GUV} are the radii of the pipette and the GUV respectively (Evans and Rawicz, 1990). A membrane nanotube was formed by pulling away a micropipette aspirated GUV whose membrane was attached to a streptavidin-coated bead (3.05 μm diameter, Spherotech, Lake Forest, Illinois, USA) held in a fixed optical trap. The custom-made optical trap was made by focusing an ytterbium fiber laser (IPG laser, Burbach, Germany) through a 100X 1.3 NA oil immersion objective (Nikon, Tokyo, Japan). The force F exerted on the bead was calculated from the Hooke's law: $F = k^*\Delta x$ where k is the stiffness of the trap ($k = 360\text{pN}.\mu\text{m}^{-1}.\text{W}^{-1}$) calibrated by viscous drag method (Neuman and Block, 2004) and Δx the displacement of the bead from its equilibrium position in the optical trap. Video-rate movies and displacement measurements were done via a C-MOS Camera (Pixelink, Ottawa, Canada) with a user-made video recorder and bead tracking software under Matlab.

Dynamin and GTP were injected close to the nanotube with a second micropipette of typical 10 micron radius controlled with a hydraulic micromanipulator (Narishige, Tokyo, Japan). Nanotubes were observed simultaneously by bright field imaging and by dual-color confocal microscopy ($\lambda_1 = 488 \text{ nm}$ and $\lambda_2 = 543 \text{ nm}$) on a Nikon eclipse Ti inverted microscope (Nikon, Tokyo, Japan). For fast 2-colors confocal experiments, a spinning disk (Intelligent Imaging Innovations, Denver, CO) and a two-channel simultaneous-imaging system (Dual-View, Photometrics, Tucson, AZ) were used instead of standard confocal microscopy (Eclipse C1 Confocal, Nikon, Tokyo, Japan).

Membrane Sheets and Dynamin Tubules Formation

To form membrane sheets, 22x40 mm glass coverslips were first cleaned by sonication (5 min) in 1% Decon 90, Modec, USA, in distilled water. After thorough washing and sonication (5 min) in distilled water to remove any trace of detergent, coverslips were finally washed with 100% ethanol prior to storage in ethanol. Coverslip were dried under a N₂ flux, and 1 μl droplets of lipid solution (10 mg/ml in pure chloroform) were deposited and allowed to dry on the coverslip. Typically, two drops were deposited at different sites on a same coverslips. The use of pure chloroform was essential to allow lipid droplet drying in a way that was optimal for the subsequent formation of membrane sheets upon hydration. Coverslips were then dried again under vacuum (0.2 milli-torr) for at least one hour, and kept up to several days under vacuum.

Before use, coverslips were placed for 20–30 min in a wet incubator (37°C, 100% humidity) to allow partial hydration of the lipids. Next, a small chamber (approximately 15 µl volume) was built by placing the coverslip onto a glass slide, with the lipids facing the glass slide, using a double-sided Scotch (3M) tape as a spacer. The lipids were fully rehydrated by applying to the side of the chamber 15–20 µl of GTPase buffer (20 mM HEPES pH 7.4, 100 mM NaCl, 1 mM MgCl₂) containing 0.1 mg/ml casein (C7078, Sigma) (casein buffer) which were taken up into the chamber by capillarity. Lipid deposits then transformed into membrane sheets. Dynamin solution, typically 0.5–1 mg/ml was then added to the side of the chamber, and transferred into the chamber by capillarity. Membrane sheets were then deformed into dynamin-coated tubules visible by DIC (Morlot et al., 2010; Roux et al., 2006).

Torque Measurement by Viscous Drag

Streptavidin beads (1.35 µm diameter streptavidin-coated, polystyrene beads, Spherotec, Lake Forest, IL) were grafted onto biotinylated dynamin tubules formed from membrane sheets (Morlot et al., 2010; Roux et al., 2006) by adding them to the chamber after tubule growth. The beads rotate following GTP addition and resulting constriction of the dynamin coat (Morlot et al., 2010; Roux et al., 2006), experiencing a viscous torque $\Gamma_v = 14\pi\eta(R+r)^3 \omega = \xi\omega$ (Happel and Brenner, 1983), where η is the viscosity of the surrounding fluid, R the radius of the bead, r the radius of the tubule and ω is the angular spinning velocity. Differential Interference Contrast (DIC) and computer-based live recording of the rotating beads with a GUPPY camera (Allied Vision Technologies, Stadtroda, Germany) allowed direct measure of the angular spinning velocity and estimation of the viscous torque from the formula above.

Stall Torque Measurement by Magnetic Field

To measure the stall torque Γ_s that arrests the constriction of the membrane tube, we use a magnetic bead, to which an external torque via a variable magnetic field. The observation chamber (Figure S2A) is placed on the stage of an Axiovert 100 microscope (Zeiss, Oberkochen, Germany) equipped with a differential interference contrast (DIC), a fluorescence lamp and a UI-2220SE charge-coupled-device (CCD camera - IDS, Obersulm, Germany). The magnetic field to manipulate the magnetic beads is generated by two homemade electromagnets (see Figure S2B). Both the electromagnets are controlled using a NI USB-6211 multifunction data acquisition card (National Instruments, Austin, Texas, USA) and a homemade power supply. Magnets are calibrated using a DC magnetometer (AlphaLab, West Salt Lake City, UT). The bead motion is recorded and tracked using user-developed procedure under MATLAB.

To calibrate the torque induced by the magnetic field, the bead is attached to a dynamin-lipid nanotube and oriented with a magnetic field parallel to the coverslip (position “1” in the schema shown in Figure S2C, top). When the magnets polarity is switched, the bead rotates around the nanotube to follow the magnetic field and goes from position “1” to position “2.” According to Langevin’s equation, the angular speed $\omega(\theta)$ of the bead is proportional to the magnetic torque $\Gamma(\theta)$

$$\varepsilon\omega(\theta) = \Gamma(\theta) + \mu(t) = \Gamma_{\max} \sin(\theta) + \mu(t),$$

Where ε is the viscous drag of the bead, $\mu(t)$ is a thermal noise and Γ_{\max} is the torque exerted when the magnetic moment of the bead is perpendicular to the field ($\theta = \pi/2$). As the thermal noise is negligible compared to the magnetic torque, the maximal angular speed $\omega(\theta = \pi/2) = \varepsilon\Gamma_{\max}$, where $\varepsilon = 14\pi\eta(R+r)^3$ (see above [Happel and Brenner, 1983]). In our measurements η is the viscosity of the water (1 mPa·s), R is the radius of the bead (655 nm) and r is the radius of the dynamin-coated tube (25 nm). For each bead Γ_{\max} is evaluated for different magnetic fields (Figure S2C, bottom).

Alternatively, the torque is calibrated with respect to the applied magnetic field through the thermal fluctuations of the beads. According to the equipartition theorem, the mean square amplitude of angular fluctuations is:

$$\Delta\vartheta^2 = \frac{k_B T}{\kappa_\Gamma},$$

where k_B is the Boltzmann constant, T is the temperature and $\kappa_\Gamma = -\partial\Gamma/\partial\vartheta|_{\Gamma=0}$ is the curvature of the magnetic potential around its minimum. The magnetic dipole moment is evaluated for different magnetic field B to obtain the calibration curve $\Gamma(B, \theta)$.

Cell Transfection, Treatment, and Imaging

COS-7 cells were transfected using FuGENE-6 (Roche Applied Science, Indianapolis, IN) with dynamin 2 fused to Green Fluorescent Protein (GFP) (kindly provided by P. De Camilli; HHMI, Yale University) or mouse clathrin-light-chain fused to mCherry or GFP (kindly provided by C. Merrifield, Cambridge and by P. De Camilli, HHMI, Yale University). Cells were imaged 18 to 24 hr post transfection in Leibovitz medium (GIBCO, Life Technologies, Paisley, UK). While imaging, the medium was changed with a hypertonic solution of 0.25 M sucrose in Leibovitz medium. Cell membrane staining was achieved by incubating cells for 5' at 37°C with deep red Cell Mask (Molecular Probes, Life Technologies, Paisley, UK) before imaging. Genome edited SK-MEL-2 cells expressing dynamin2-GFP and clathrin Light Chain-RFP were provided by D.G. Drubin (University of California Berkeley, USA).

Transferrin Labeling

Cells were starved in serum deprived DMEM-F12 medium for 30 min on ice, then incubated with 5 µg/ml Alexa-fluor 594 Transferrin (Invitrogen) in hypertonic medium (0.25 M sucrose Leibovitz medium) for 3' at RT. Cells were washed with hypertonic buffer before imaging.

Image Analysis

Images were analyzed and processed with ImageJ. Kymographs were made with Multiple Kymograph plugin (J. Rietdorf; A. Seitz). Fits were made with the curve fitting toolbox in Matlab.

Membrane Shape Computation

In this section we first derive the equilibrium equation for the shape of the membrane from Canham-Helfrich Hamiltonian and express the shape computation as a boundary value problem suitable for solution with Matlab's bvp4c.

Canham-Helfrich Hamiltonian gives the energy of the membrane as a function of its shape:

$$E = \sigma \int dA + \frac{\kappa}{2} \int J^2 dA.$$

The first term is related to the energy cost of stretching the membrane and σ is the membrane tension which can be controlled in the experiment. The second term represents the energy cost of bending which is given by the integral of membrane curvature J over the surface. The bending modulus κ depends on the composition of the membrane.

Considering the axial symmetry of the experiment we will restrict ourselves to axisymmetric shapes. For an axisymmetric surface with an axial coordinate z , and angle φ around the z axis, and a radius $r(z)$, curvature can be expressed as:

$$J = \frac{r(z)r''(z) - r'(z)^2 - 1}{r(z)(1 + r'(z)^2)^{3/2}}.$$

Writing the area element in the same coordinates $dA = r(z)\sqrt{r'(z)^2 + 1}dzd\varphi$, the integral in the angle φ can be directly performed and the energy can be cast in the following form:

$$E = \int \left(\sigma + \frac{\kappa}{2}J^2\right)r(z)\sqrt{r'(z)^2 + 1}dz = 2\pi \int \left(\sigma + \frac{\kappa}{2}J^2\right)r(z)\sqrt{r'(z)^2 + 1}dz.$$

It will be convenient for numerical solution of the equations to nondimensionalize the Hamiltonian using the bare membrane radius $R_m = \sqrt{\kappa/2\sigma}$ to rescale all lengths, and $\pi\kappa$ to rescale the energy:

$$e = \int (1 + j^2)\rho(\theta)\sqrt{\dot{\rho}(\theta)^2 + 1}d\theta = \int \ell(\rho(\theta), \dot{\rho}(\theta), \ddot{\rho}(\theta))d\theta,$$

where

$$j = \frac{\rho(\theta)\ddot{\rho}(\theta) - \dot{\rho}(\theta)^2 - 1}{\rho(\theta)(1 + \dot{\rho}(\theta)^2)^{3/2}}, \rho(\theta) = \frac{r(z)}{R_m}, \theta = \frac{z}{R_m}, e = \frac{E}{\pi\kappa}, \ell = (1 + j^2)\rho(\theta)\sqrt{\dot{\rho}(\theta)^2 + 1}$$

are all adimensional quantities and the dot represents differentiation with respect to θ . At equilibrium, membrane shape minimizes the energy. Thus, the equilibrium shape is given by the solution of Euler-Lagrange equation

$$\frac{d\ell}{d\theta} = \frac{d}{d\theta} \frac{\partial \ell}{\partial \dot{\rho}} - \frac{d^2}{d\theta^2} \frac{\partial \ell}{\partial \ddot{\rho}},$$

which is the nonlinear fourth order differential equation:

$$\begin{aligned} & \left(-1 - 6\dot{\rho}^2 - 10\dot{\rho}^3 - 9\dot{\rho}^4 - 10\dot{\rho}^5 - 4\dot{\rho}^6 + \rho\ddot{\rho}(3 + 30\dot{\rho} - 9\dot{\rho}^2 - 40\dot{\rho}^3 - 12\dot{\rho}^4) + \rho^2(1 + \dot{\rho}^2)(1 + \dot{\rho}^4 + \dot{\rho}^6 + 3\dot{\rho}^2 + \dot{\rho}^2(3 - 12\dot{\rho}^2) \right. \\ & \left. + 4\dot{\rho}\ddot{\rho} + 4\dot{\rho}^3\ddot{\rho}) + \dot{\rho}^3 \left(5(-1 + 6\dot{\rho}^2)\ddot{\rho}^3 - (1 + \dot{\rho}^2)\ddot{\rho}(1 + 2\dot{\rho}^2 + \dot{\rho}^4 + 20\dot{\rho}\ddot{\rho}) + 2(1 + \dot{\rho}^2)^2\ddot{\rho} \right) \right) = 0 \end{aligned}$$

This equation was solved in the domain $\theta \in [0, 10]$, with two different sets of boundary conditions. For the junction between the tube and the dynamin-coated tube, it was required that

$$\rho(0) = 1, \dot{\rho}(0) = 0$$

$$\rho(10) = r_d, \dot{\rho}(10) = 0$$

with $r_d = R_d/R_m$ the adimensional dynamin radius, which was varied to compute the energy at different levels of constriction.

For the neck joining the vesicle or bead to the dynamin-coated tube, boundary conditions were

$$\rho(0) = 20, \rho(0)\ddot{\rho}(0) - \dot{\rho}(0) - 1 = 0$$

$$\rho(10) = r_d, \dot{\rho}(10) = 0.$$

The first condition ensures membrane joins the flat wall that mimics the vesicle at $\theta = 0$ with vanishing curvature. See the following parts of the [Extended Experimental Procedures](#) for more details on the rationale for these boundary conditions.

Boundary conditions for the vesicle geometry do not directly produce a solution with Matlab's bvp4c boundary value problem solver. A technique known as *continuation* was used to find the desired solution. The solution for a less *stringent* boundary condition (i.e., giving a less bent membrane) with $\rho(0) = 7, \rho(10) = 1$ was first computed and used as initial guess for a subsequent iteration with a slightly greater value of $\rho(0)$. This process was then repeated until the desired $\rho(0) = 20$ condition was met. Finally, the same process was used to decrease $\rho(10)$ from 1 to the desired value r_d .

Once membrane shapes were computed, we calculated the corresponding energy by numerical integration of Canham-Helfrich Hamiltonian.

Theory for Reduced Fission Energy Barrier at the Dynamin-Membrane Edge

We model membrane fission as a one-step reaction thermally activated with a single energy barrier, biased by the GTP hydrolysis driven constriction force. The radius R_d , that is, the radius of the dynamin-coated membrane, constitutes the reaction coordinate. In this analogy, the radius R_d is a brownian degree of freedom that may overcome a fission energy barrier by thermal fluctuations. GTP hydrolysis by dynamin generates a constriction force which in our model would operate as a force on the R_d degree of freedom, tilting the energy landscape and decreasing the total energy barrier ΔE_{tot} to a smaller value ΔE_{res} , biasing the transition toward the fission state (see [Figure 2A](#) in main text).

The energy barrier originates from differences in elastic and surface energy of the membrane neck that joins the edge of the dynamin-coated part to the bare tube with radius R_d , set by tension and bending rigidity.

After constriction, the residual barrier can be overcome by thermal fluctuations of the constricted radius, at a rate

$$r = \tau^{-1} e^{-\Delta E_{\text{res}}/k_b T}$$

where τ is a molecular characteristic time of reaction, k_b is the Boltzmann constant, T the temperature. A constant rate of reaction yields an average fission time

$$\langle t_f \rangle = \tau e^{\Delta E_{\text{res}}/k_b T}$$

A process with just one constant rate of reaction r gives an exponential distribution of reaction times

$$\rho(t_f) = r e^{-rt_f}$$

and consequently a cumulative probability of reaction

$$F(t_f) = \int_0^{t_f} \rho(x) dx = 1 - e^{-rt_f}.$$

Our experiments both present an exponential distribution of fission times (data not shown) and the corresponding cumulative probability is well fit by $1 - e^{-rt_f}$ as shown in [Figure 3B](#) in the main text.

To compute the bending and surface energy of the membrane we numerically solved the nonlinear shape equation that arises from Canham-Helfrich Hamiltonian minimization (see above) for the neck joining a bare membrane tube with a dynamin-coated one (see [Figure 1G](#) in the main text). This implies boundary conditions where the radius matches the bare tube radius R_m on one side and R_d , the radius of the dynamin-coated part, on the other. In both ends, the derivative of the radius with respect to the axial coordinate must vanish to smoothly join either the bare or dynamin-coated tube. The equation was numerically solved using Matlab bvp4c boundary problem solver for different values of R_d and constant R_m . From the shape, we compute the bending and surface energy energy $E(\alpha)$ as a function of dimensionless parameter $\alpha = R_m/R_d$, as depicted in [Figure 2B](#).

To estimate the energy barrier we assume dynamin polymerizes and constricts the dynamin-coated membrane very fast compared to fission times ([Morlot et al., 2010](#)) to a radius R_c of the order of 4-5nm in the presence of GTP (the actual R_c should depend on GTP concentration in our model as fission time decreases with increasing GTP concentration; we nevertheless disregard this dependence for the sake of simplicity by taking a fixed GTP concentration and defer the discussion on the effect of GTP concentration for a later section). The coated membrane tube is still connected to the bare membrane tube by a neck-like shape. In order for the membrane to break, it makes a transition from this configuration with $R_d = R_c$, to another with a constricted radius $R_d = R_i$ corresponding to a hemifission intermediate state with a radius R_i independent of tension and bending rigidity. A hemifission intermediate is a state where the internal monolayer of the membrane is fused while the outer monolayer keeps its integrity. Evidence for the existence of a hemifission state has already been reported in ([Bashkirov et al., 2008](#)). Kozlovsky and Kozlov have proven for a different but related geometry where a constricted neck also exists that once this hemifission intermediate is attained the transition to complete fission proceeds spontaneously, due to a negative free energy difference between hemifission and complete fission state ([Kozlovsky](#)

and Kozlov, 2003). We assume there is no barrier once the hemifission is attained and therefore the fission reaction quickly proceeds to fission.

Hence, the energy barrier is the difference between the energy of these two configurations

$$\Delta E_{\text{res}}^{\text{tube}} = E\left(\frac{R_m}{R_i}\right) - E\left(\frac{R_m}{R_c}\right) \equiv E_i^{\text{tube}} - E_c^{\text{tube}}.$$

Taking R_i of the order of 3-5nm and R_c in the range 4-5nm and for the R_m used in our experiment, the ratio α ranges from 1 to 10, which allows us to approximate $E(\alpha)$ by a straight line with slope $\alpha \approx 1/4$ and get an analytical prediction of the barrier dependence with tension and bending modulus

$$E \approx a 2\pi \kappa (\alpha - 1) \Rightarrow \Delta E_{\text{res}}^{\text{tube}} \approx 2\pi a \left(\frac{1}{R_i} - \frac{1}{R_c} \right) \frac{\kappa^{3/2}}{\sqrt{2\sigma}},$$

where we already substituted the value of the bare membrane radius $R_m = \sqrt{\kappa/2\sigma}$. The average fission time thus depends on membrane parameters as

$$\langle t_f \rangle = \tau e^{\frac{b\kappa^{3/2}}{k_b T \sqrt{\sigma}}}$$

giving for $\log \langle t_f \rangle$ a dependence

$$\log \langle t_f \rangle = \log \tau + \frac{b\kappa^{3/2}}{k_b T \sqrt{\sigma}},$$

which fits all the experimental data for different values of κ and σ as shown in Figure 3 in the main text.

Fission at GUV-Dynamin or Bead-Dynamin Edge

As explained in the main text, fission occurs preferentially at the boundary between the tube and the GUV or between the tube and the bead. To analyze these cases we solved the shape equation with a modified boundary condition at GUV/bead's end. Due to the difference in size between the tube and the bead or GUV we can approximate GUV/bead by an infinite flat membrane wall perpendicular to the tube. This can be mimicked in the numeric computations by requiring that membrane radius at the wall (GUV) is much bigger than R_d and that membrane joins smoothly to a flat membrane, i.e., with vanishing curvature. At dynamin's edge, membrane has a radius R_d and enters the dynamin domain with vanishing slope to smoothly match the dynamin-coated tube. The dynamin coating is assumed to progress until a distance $10R_m$ from the flat wall. This coincides with the end of the bare tube that would form in the absence of dynamin (Derényi et al., 2002) and we expect the dynamin polymer to grow approximately until that position. Varying R_d again we can compute the energy as a function of α . The energy of the GUV-dynamin edge has the same approximate shape as in the bare tube-dynamin case (see Figure 2B) and therefore the above discussion remains valid, giving a similar dependence with κ and σ for fission time. Furthermore, the residual energy barrier for the vesicle or bead edge for $\kappa = 16k_b T$, $R_i = 3\text{nm}$ and $R_c = 4.5\text{nm}$ ranges from $20 k_b T$ to $23 k_b T$ as a function of tension σ giving an expected fission time

$$\langle t_f \rangle = \tau e^{\frac{\Delta E_{\text{res}}^{\text{ves}}}{k_b T}},$$

which agrees with experimentally observed times. Using hydrodynamic arguments we can estimate $\tau \approx 10^{-9}\text{s}$ giving in turn fission times in the range [1, 13]s depending on tension, in agreement with experimental fission times.

Higher Probability of Fission at GUV's End

Differences in energy barrier for fission at the GUV-dynamin and at the tube-dynamin neck translate in different rates of fission. Disregarding differences in the number of tube-dynamin versus GUV-dynamin edges in front of the exponential factors, the probabilities to find a break in the GUV or tube edge in an experiment would be proportional to the rates of fission. According to our model, rates are exponentially related and therefore:

$$\frac{P_{\text{ves}}}{P_{\text{tube}}} = \frac{e^{-\Delta E_{\text{res}}^{\text{ves}}/k_b T}}{e^{-\Delta E_{\text{res}}^{\text{tube}}/k_b T}} = e^{(\Delta E_{\text{res}}^{\text{tube}} - \Delta E_{\text{res}}^{\text{ves}})/k_b T}$$

with $\Delta E_{\text{res}}^{\text{tube}}$ and $\Delta E_{\text{res}}^{\text{ves}}$ the barriers for fission at the tube or vesicle respectively. Using normalization $P_{\text{ves}} + P_{\text{tube}} = 1$ we find

$$P_{\text{ves}} = \frac{1}{1 + e^{(\Delta E_{\text{res}}^{\text{ves}} - \Delta E_{\text{res}}^{\text{tube}})/k_b T}}.$$

Taking $R_i = 3\text{nm}$, $R_c = 4.5\text{nm}$ and $\kappa = 16k_bT$, the numerical computation of the barriers from the surface and bending energy shows that the energy barrier at the vesicle edge is always smaller than the barrier corresponding to the tube, at least for the values of tension used in the experiment, as shown in [Figure 2C](#). For tensions used in experiments from $\sigma = 1 \times 10^{-4} \text{ N.m}^{-1}$ to $\sigma = 5 \times 10^{-4} \text{ N.m}^{-1}$, the difference in energy barriers $\Delta E_{\text{res}}^{\text{tube}} - \Delta E_{\text{res}}^{\text{ves}}$ is in the range $[1, 3] \times k_bT$, which in turn gives probabilities of fission in the vesicle $P_{\text{ves}} = [0.75, 0.93]$ in accordance with 75% of the breaks occurring in the vesicle observed in experiment (see [Figure 1D](#)).

Effect of GTP Concentration

The presence of GTP in the system, which entails dynamin contraction, is equivalent, at least for small deformations of the helix, to applying a homogeneous constriction force or pressure and a torque to the membrane in the dynamin domain proportional to $\Delta\mu$, the GTP hydrolysis chemical potential difference ([Lenz et al., 2008](#)). In our model, that would mean that a constant force is applied to the radius variable, which can be seen as a tilt in the energy landscape proportional to $\Delta\mu$. Thus, the total energy barrier decreases in an amount proportional to $\Delta\mu$ with a constant d that is related to the position of the intermediate state in the reaction path:

$$\Delta E_{\text{res}} = \Delta E_{\text{tot}} - d\Delta\mu = \Delta E_{\text{tot}} - c\Gamma\theta,$$

where we used the proportionality between $\Delta\mu$ and dynamin induced torque upon hydrolysis Γ , which is derived assuming the energy for constriction is coming from GTP hydrolysis and thus work done by dynamin should be $\Gamma\theta = \xi\Delta\mu$ where $\Delta\mu$ is the variation of chemical potential in the hydrolysis and ξ can be thought of as an efficiency of dynamin in the sense of how much energy is converted into work.

This gives for fission time

$$\langle t_f \rangle = \tau e^{\frac{\Delta E_{\text{tot}}}{k_b T} - c\frac{\Gamma\theta}{k_b T}}.$$

Finally, assuming an ideal dynamin solution, $\Delta\mu = k_b T \log[GTP]$ and therefore

$$\langle t_f \rangle = \tau e^{\frac{\Delta E_{\text{tot}}}{k_b T} - c\xi \log[GTP]}.$$

Experiments indeed show the expected dependence: $\log(t_f) = \text{constant} - c\xi \log[GTP]$ as shown in [Figure 4F](#) of the main text.

Torque and Final Helix Radius

As the dynamin helix hydrolyses GTP, it exerts a torque which tends to constrict the underlying membrane tubule. This torque is counteracted by the elasticity of the membrane, which favors a widening of the tubule. Here we derive a mathematical expression for the membrane's radius resulting from the balance of these two effects. We consider a cylindrical membrane constrained by a dynamin helix and first consider the geometrical relationships between the helix' radius, pitch and length. We then use them to analyze the competition between dynamin torque and membrane elasticity.

We approximate the dynamin helix by an inextensible ribbon wound around a cylinder of radius r and length L . No polymerization or depolymerization is assumed to take place over the time scales considered and the ribbon has an approximately constant width. Therefore, the total surface area of the ribbon is conserved:

$$2\pi rL = 2\pi R_u L_u,$$

where the index u refers to the initial state of the helix, prior to the introduction of GTP, when the dynamin helix is unconstrained. We define Θ as the total winding angle of the ribbon, expressed in radian. For instance, a helix that winds three times around the cylinder has $\Theta = 3 \times (2\pi)$. Denoting by h the helix' pitch, this angle is given by

$$\frac{\Theta}{2\pi} = \frac{L}{h}$$

expressing the fact that adding one turn to the helix increases its length by h . To the level of approximation used here, we can assume that the pitch of the helix is constant and equal to 10nm.

We denote by κ the bending modulus of the membrane and assume that the tubule is in contact with a membrane reservoir of tension σ . Due to the small radius of the tubule (much smaller than the bare membrane equilibrium radius $\sqrt{\kappa/2\sigma}$), the energetic contribution of surface tension is small compared to the bending energy, and is neglected in the following.

The bending energy of the membrane is given by the Canham-Helfrich energy presented in the main text. Its bending term is reproduced here for convenience:

$$E_{\text{bending}} = \frac{\kappa}{2} \int_A c^2 dA.$$

For a cylindrical geometry, the curvature of the tube is $c = 1/r$ and the integral runs over a surface $A = 2\pi rL$. The bending energy thus reads $\pi\kappa L/r$, which is minimal for a flat membrane ($r \rightarrow +\infty$). In the absence of GTP hydrolysis, the membrane is confined to a finite radius R_u by the rigidity of the dynamin helix. We represent this passive effect by an elastic equilibrium torque Γ_u implying a contribution $-\Gamma_u\Theta$ to the energy of the system.

For the purpose of determining the membrane shape, the internal, active torque induced by the dynamin polymer upon GTP hydrolysis is equivalent to an additional external torque Γ imposed on the passive helix. Therefore, dynamin activity can be described as a further lowering of the energy of the system by an amount equal to the work $\Gamma\Theta$ of this torque. Summing all the contributions to the energy, we find

$$E = -(\Gamma_u + \Gamma)\Theta + \pi\kappa \frac{L}{r} = -(\Gamma_u + \Gamma) \frac{L_u R_u}{hr} + \pi\kappa \frac{L_u R_u}{r^2}.$$

Minimizing E with respect to r , we find that

$$r = \frac{2\pi\kappa h}{\Gamma_u + \Gamma}.$$

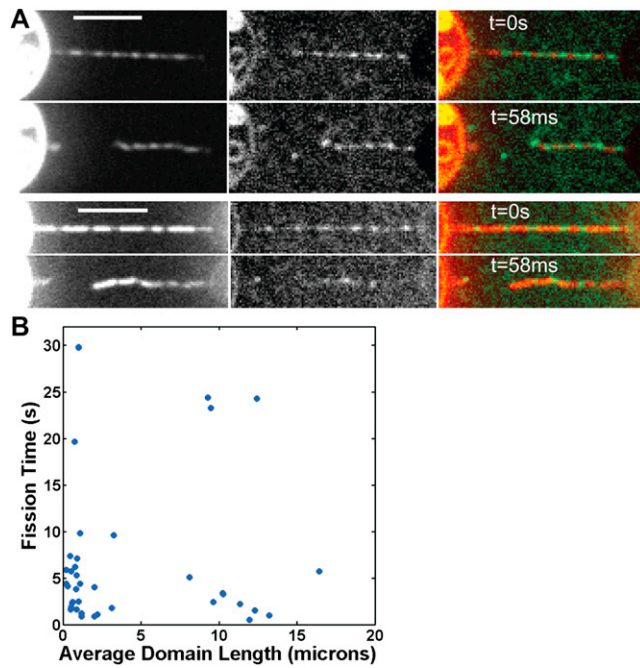
While the passive torque Γ_u has been left unspecified until this point, it must satisfy the condition that r goes to R_u as Γ goes to zero. This implies that $\Gamma_u = 2\pi\kappa h/R_u$, and therefore

$$r = \frac{R_u}{1 + \frac{\Gamma R_u}{2\pi\kappa h}}.$$

Using $\kappa = 20 \text{ kbT} = 8 \times 10 - 20 \text{ J}$, we can thus compute the torque required to obtain a constricted radius $r = R_c = 5 \text{ nm}$ to be $\Gamma \approx 500 \text{ pN.nm}$. This value is compatible with the experimental measurements presented in the main text (see [Figure 4](#)), thus validating our assessment of the role of the competition between dynamin torque and membrane bending rigidity.

SUPPLEMENTAL REFERENCES

- Derényi, I., Jülicher, F., and Prost, J. (2002). Formation and interaction of membrane tubes. *Phys. Rev. Lett.* **88**, 238101.
- Neuman, K.C., and Block, S.M. (2004). Optical trapping. *Rev. Sci. Instrum.* **75**, 2787–2809.
- Stowell, M.H., Marks, B., Wigge, P., and McMahon, H.T. (1999). Nucleotide-dependent conformational changes in dynamin: evidence for a mechanochemical molecular spring. *Nat. Cell Biol.* **1**, 27–32.



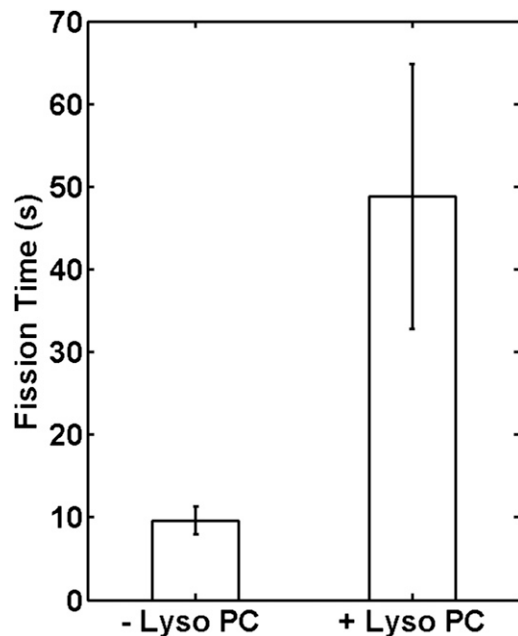


Figure S2. Fission Is Delayed by Lysolipids, in Agreement with the Hypothesis of a Hemifission Intermediate, Related to Figure 2

Histogram of average fission times for two lipid compositions: 80% EPC + 19%PIP₂ + 1%RedPIP₂ (-Lyo PC) and 50% EPC + 30% Lyso PC + 19%PIP₂ + 1%RedPIP₂ (+Lyo PC). Error bars represent SEM. The same concentrations of dynamin (2.5 μM) and GTP (150 μM) were used for both experiments. For -Lyo PC, the average fission time is $\langle t_f \rangle = 9.6 \pm 1.7$ s, N = 44. For +Lyo PC, $\langle t_f \rangle = 48.8 \pm 16$ s, N = 31. In this second case, three tubes where fission was not observed within 5 min after dynamin polymerization were taken into account, 300 s was used as an underestimate of their fission time.

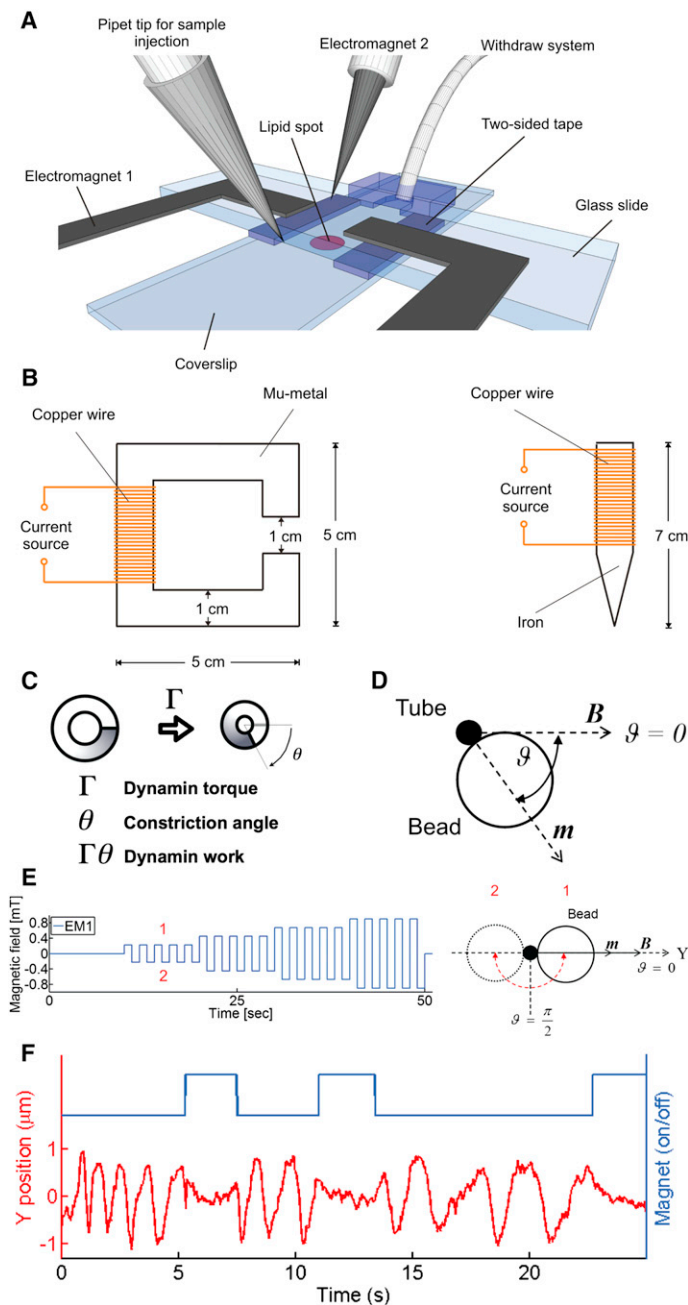


Figure S3. Dynamin Torque Counteracted by an External Torque Generated by a Magnetic Field, Related to Figure 4

(A) Schematic view of the observation chamber made of a coverslip, a glass slide and two-sided tape as a spacer. Lipids are spotted on the coverslip. The fluids are placed on one side with a pipette and withdrawn using a syringe pump from the other side of the chamber. The observation chamber is surrounded by two electromagnets EM 1 and EM 2 (dark gray) to impose a controlled magnetic field.

(B) Left: EM 1 is about 1 mm thick and consists of a coil of insulated copper wire wrapped around a mu-metal core. Right: EM 2 consists of a coil of insulated copper wire wrapped around an iron tube (1 cm diameter) with a tip to focus the magnetic field.

(C) Sketch representing dynamin torque and constriction angle.

(D) Sketch of the magnetic bead bound to the tube.

(E) Right: a schematic view of the magnetic bead bound to the membrane tube (in black). When the magnets polarity is switched, the bead passes from one side of the tube to the other. The maximum angular speed of the bead is proportional to the maximum value of the applied torque. Left: typical magnetic field profile used for torque calibration.

(F) Y-position trace (red curve) of a magnetic bead attached to a dynamin-coated tube (see Movie S5) upon GTP hydrolysis manipulated with magnetic tweezers illustrated by the blue rectangular function where the lower line marks the state of zero field ("off") and the upper line the state of an applied constant field of 4 mT ("on").

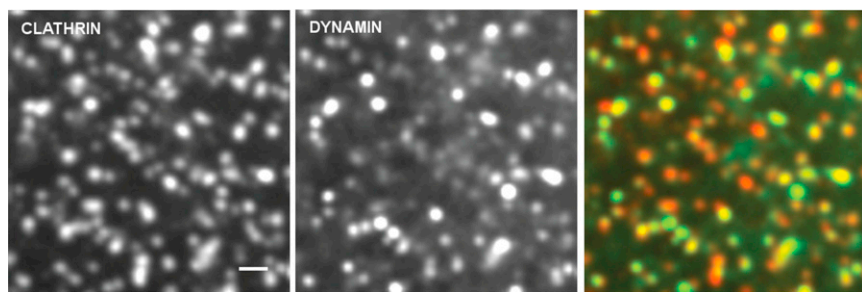


Figure S4. Dynamin and Clathrin Colocalize in Live Cells, Related to Figure 5

Colocalization of clathrin-RFP and dynamin-GFP in genome edited SKML-2 cells. Scale bar, 1 μ m.

Table S1. Fission Times Follow an Exponential Distribution, Related to Figure 3

GTP Concentration (μ M)	Average Fission Time (s)	Fitted Time Parameter τ (s)
10000	6.2 \pm 0.8	6.22 (3.78, 8.65)
500	9.8 \pm 1.1	9.56 (8.50, 10.62)
100	14.2 \pm 1.7	19.62 (14.87, 24.37)
50	18.7 \pm 0.3	27.73 (25.47, 30)
10	44.8 \pm 20.8	31.47 (22.66, 40.29)
5	52.6 \pm 17.4	48.41 (41.72, 55.1)
1	85.3 \pm 8.7	89.75 (60.45, 119.2)

Fission times were measured for several tubes at different concentrations of GTP. The average fission time (center column, mean+SEM) is similar to the parameter τ given by an exponential fit of the fission time distribution (right column, fitted parameter and 95% confidence interval), which is characteristic of an exponential distribution (see also Figure 3B).

Table S2. Cholesterol and Sphingomyelin Rigidify Membranes, Related to Figure 3

Lipid Composition	Bending Rigidity ($k_B T$)
80% EggPC + 20% PI(4,5)P ₂	16.2 \pm 1.2
70% EggPC + 10% BSM + 20 %PI(4,5)P ₂ , 40% Cholesterol	23.5 \pm 3.7
80% EggPC + 20% PI(4,5)P ₂ , 50% Cholesterol	25 \pm 2.4
80% BSM + 20% PI(4,5)P ₂ , 50% Cholesterol	40.2 \pm 5.4

Average bending rigidity and SEM for different lipid compositions. The bending rigidity of a GUV was calculated from the relationship between force and tension. The proportions of PIP₂ is the same for all compositions. These four lipid compositions were used to test the dependence of fission time on bending rigidity (see Figure 3C).